

Paleoceanography of the Strait of Hormoz and its link to paleoclimate changes since the mid-Holocene

Mohammad Ali Hamzeh, Maziar Khosravi, Xavier Carton, Dariush Yarahmadi, Ezatollah Safarkhani

▶ **To cite this version:**

Mohammad Ali Hamzeh, Maziar Khosravi, Xavier Carton, Dariush Yarahmadi, Ezatollah Safarkhani. Paleoceanography of the Strait of Hormoz and its link to paleoclimate changes since the mid-Holocene. CONTINENTAL SHELF RESEARCH, 2021, 226, 10.1016/j.csr.2021.104507 . insu-03683257

HAL Id: insu-03683257

https://insu.hal.science/insu-03683257

Submitted on 14 Apr 2023

HAL is a multi-disciplinary open access archive for the deposit and dissemination of scientific research documents, whether they are published or not. The documents may come from teaching and research institutions in France or abroad, or from public or private research centers.

L'archive ouverte pluridisciplinaire **HAL**, est destinée au dépôt et à la diffusion de documents scientifiques de niveau recherche, publiés ou non, émanant des établissements d'enseignement et de recherche français ou étrangers, des laboratoires publics ou privés.

Continental Shelf Research
September 2021, Volume 226, Pages 104507 (15p.)
https://doi.org/10.1016/j.csr.2021.104507
https://archimer.ifremer.fr/doc/00705/81735/

Archimer
https://archimer.ifremer.fr

Paleoceanography of the Strait of Hormoz and its link to paleoclimate changes since the mid-Holocene

Hamzeh Mohammad Ali [1, *], Khosravi Maziar [1], Carton Xavier [2], Yarahmadi Dariush [3], Safarkhani Ezatollah [3]

[1] Iranian National Institute for Oceanography and Atmospheric Science (INIOAS), No.3, Etemad Zadeh St., Fatemi Ave., Tehran, IR, Iran
[2] Laboratory for Ocean Physics and Satellite Remote Sensing (LOPS), UMR6523, Ifremer, Univ. Brest, CNRS, IRD, Brest, France
[3] Department of Geography, Faculty of Literature and Humanities, Lorestan University, Khorramabad, Iran

* Corresponding author : Mohammad Ali Hamzeh, email address : Hamzeh@inio.ac.ir

Abstract :

This paper presents the paleocurrent evolution of the Persian Gulf deep water (PGDW) during the last 5000 years using faunal (foraminiferal assemblage) and non-faunal (magnetic susceptibility, sediment grain size, number of coarse relict particles and physicochemical characteristics) indicators from a 133 cm long core retrieved from the Strait of Hormoz (SH). Our results suggest that the precession-related insolation change and solar variability induced long-term and short-term sea surface temperature (SST) rise and fall resulted in variation of PGDW outflow strength. Two periods of decreasing SST (5000–4300 and 2000–1450 cal yr BP), accompanied by wetter conditions in the Middle East, are related to the reduction of the PGDW current velocity. A combination of high sedimentation rate (0.72 mm yr−1, due to high terrigenous input) with a relatively low bottom flow energy cause the settling of finer sediments providing a favourable environment for the expansion of benthic foraminifera (dominated by infaunal taxa). On the contrary, the PGDW current velocity strengthens in the periods of SST increase (4300–2000 and 1450 cal yr BP to present) with decreasing sedimentation rate (0.15–0.34 mm yr−1, due to low river discharge). During both periods of high-velocity bottom currents, the benthic foraminifera accumulation rate decreases. However, as the PGDW brings a relatively high amount of dissolved oxygen (3.25 mg/l in summer and 4.79 mg/l in winter) and phytodetritus particles, compared to the surrounding water, some particular foraminifera (especially robust suspension feeder epifaunal taxa) evolved. SST increase, intensified by anthropically caused global warming, may lead to PGDW intensification in the future.

Please note that this is an author-produced PDF of an article accepted for publication following peer review. The definitive publisher-authenticated version is available on the publisher Web site.

Highlights

► Since the mid-Holocene, PGDW intensity has been under influence of the continental climate of SW Asia and the Arabian Sea SST. ► SST intensification (4500 to 3000 and 1400 cal yr BP to present), causes increasing bottom current energy of the Strait of Hormoz and decreasing river discharges. ► Although high energy bottom currents provide a hostile environment for the benthic fauna, it brings high DO content bottom waters.

Keywords : Benthic foraminifera, Persian Gulf deep water, Relict sediments, SST, Terrigenous input

Please note that this is an author-produced PDF of an article accepted for publication following peer review. The definitive publisher-authenticated version is available on the publisher Web site.

1. Introduction

The Strait of Hormoz (SH), also called Strait of Hormuz, is a well-known 55 to 95 km wide channel linking the Persian Gulf (PG) with the Gulf of Oman and the Arabian Sea, and also, separates Iran (in the north) from the Arabian Peninsula (in the south). This waterway is of great strategic and economic importance, especially as about one-fifth of the world's oil supply and one-third of liquefied natural gas collected from various ports on the PG passes through the strait (Sheppard et al. 2010). On the other hand, SH bottom is the passageway of the Persian Gulf deep water (PGDW) (Johns et al. 2003). This strait plays a critical role in determining the circulation in the PG by constricting the water exchange between the PG and the open ocean. The PGDW outflow descends across the shelf in the northern Gulf of Oman, entrains ambient fresher water and is intensively diluted (Wyrtki 1971). Undoubtedly, climate change plays a fundamental role in determining the outflow regime by altering the contrast in physical properties of two water bodies separated by the SH (Yao and Johns 2010; Bower et al. 2000).

Lying at the transition zone between the Mediterranean winter rain (whose route is controlled by Mid Latitude Westerlies (MLW)) and the Indian Summer Monsoon (ISM) domains, the SH has experienced various climatic regimes during the Holocene (Regard et al. 2006; Arz et al. 2003). The relative influence of the above components of atmospheric circulation patterns is dependent on variations in the mean latitudinal position of the Inter-Tropical Convergence Zone (ITCZ) (Kodera 2004). Since the mid-Holocene, precession and obliquity cycles caused a shift of perihelion from September to January and a decrease in the tilt of the Earth's axis. The resulting radiative changes caused a decrease in the summer and an increase in the winter insolation in the northern hemisphere (Lorenz et al. 2006; Kim et al. 2004). These seasonality changes in insolation caused the southward migration of ITCZ being accompanied by significant paleoclimate variations in different parts of SW Asia particularly the study area which is located within this translocation territory (Hamzeh et al. 2016; Fleitmann et al. 2007). Besides, the shallowness of this area makes its response to meteorological variables quick and dramatic (Hunter, 1986). The SH is thus an essential region for the study of the interactions between climatic changes and their effects on paleoceanography. Although continuous Holocene climate records from the Mediterranean and ISM-dominated areas allow comparing the regional climate with global climatic signals, the interaction of paleoclimate changes and paleoceanography of the PG and SH has remained unknown.

Paleoceanography studies reveal that high-energy bottom currents have strong effects on, for instance, water turbulence, suspension load, and boundary layers, which should significantly influence the sedimentology and ecological conditions at the seafloor (Zhong et al. 2017; Shimmield et al. 1994). These currents can be traced by evaluating the physical and ecological characteristics of bottom sediments (Schönfeld 1997; Hollister and Heezen 1972). In the absence of current measurements, some proxies such as grain size analysis and benthic foraminiferal assemblages could be used to estimate paleo-current variations (Schönfeld 2002a, 2002b; Hollister and Heezen 1972). Lutze and Altenbach (1988) showed that intensified bottom water currents influence the physical properties of microhabitats and composition of the benthic foraminiferal fauna as well. Studies of particle size also shed light on many facets of sea bottom depositional conditions such as relative bottom current speed (McCave 2007). In the present paper, the influence of paleoclimate on paleocurrent change of deep outflow regime in the PG and SH is evaluated by using physical characteristics and benthic foraminiferal assemblages of bottom sediments.

2. Materials and Methods

2.1. Strait of Hormoz

The strategically and economically pivotal SH connects the PG to the continental shelf in the northwestern Gulf of Oman. It is 56 km wide at its narrowest point (although its central channel is about half as wide) with a sill depth of 80 m (Kassler 1973). Geologically, the study area corresponds to the transition zone between the subduction (the Indian Ocean vs Eurasian plates) and collision (Arabian vs Eurasian plates) zones (Regard et al. 2006). The geology of the area exhibits the easternmost folds of the Zagros fold-thrust belt. The anticlines of the coastal area are capped most often by Eocene to Miocene limestone rocks, while the synclines are composed mainly of Miocene sandstone and marls as well as Plio-Pleistocene conglomerates (Molinaro et al. 2004). To the east, the structures of the Zagros Mountains suddenly change to the NNW-trending folds and thrusts of the Zendan–Minab Belt composed of a poorly consolidated Mio-Pliocene pebbly sandstone and marls (Molinaro et al. 2004).

SH contains the islands of Qeshm, Hormoz (Hormuz), Lārak and Hengām. Qeshm, the largest island of the PG, forms the northern flank of the SH and southeastern marginal foreland of the ZFTB (Fig. 1). Numerous salt diapirs containing Lower Cambrian volcano-sedimentary complex (basalt, basaltic andesite, andesite, trachyte, pyroclastics, evaporite rocks and

Precambrian sedimentary units) occur on the mainland also in the form of small islands in the PG (Taghipour and Taghipour 2009). Kuh-e-Namakdan (Mt. Saltcellar) is an instance of a salt dome being exposed in the western part of Qeshm Island (Haghipour and Fontugne 1993). During the last glacial maximum (when sea level was 120 m lower than today) until about 14000 yr BP, the entire area was a dry valley and reached its present water level about 6000 years B.P. Based on the Holocene paleoshoreline reconstruction models, the coring area was inundated about 8000 yr BP (Bruthans et al. 2006; Pirazzoli et al. 2004).

Modern bottom sediments of the PG are mostly composed of terrigenous sand components, relict sand particles and biogenic carbonates and, especially at the deeper parts, are characterized by sandy silt (sand content: 20 - 30%). At the bottom of the main channel, gravelly sand, gravelly sand and muddy sandy gravel appear. Pebble fraction in some areas reaches to more than and 30% (Hamzeh in press).

Freshwater inflow is dominated by the northern coasts (originating from Taurus and Zagros Mountains). The annual mean flow of the rivers decreases from NW to SE and is as follow: Karoon: 20, Karkheh: 5.5, Hendijan: 2, Jarrahi and Mond: 1.5, Helleh: 0.6, Mehran and Kol: 0.1 km^3 yr (Al-Said et al. 2018).

2.1.1. Climate and paleoclimate

Coastal regions of SH receive Mediterranean-type winter precipitation, in association with MLW. Because of the influence of the Siberian High, only deep depressions from the Mediterranean coast can get to the coastal area. In this area, the absence of significant topographic barriers along the MLW allows Atlantic low-pressure cells to penetrate. The warm surface waters of the PG provide subsidiary moisture sources allowing storms to maintain or reinforce as they move to the eastern PG and SH (Regard et al. 2006). During the last half-century, mean annual precipitation and mean annual air temperature the area have been about 180 mm and 27 °C respectively (IWRMC, 2016). During the summer, the moist MLW moves northward and hot and dry weather prevails. Due to low pressures over southern Asia, the prevailing winds are thus northerly and northwesterly (such as the dominant northwesterly wind known as “Shamal” which enhances dust phenomena particularly in summer months) and the ITCZ lies at its northernmost position (the extreme south of Iran). However, the SH region remains beyond the influence of Indian monsoon (Fig. 1) (Regard et al. 2006). Below the ITCZ, prevailing winds are westerly and southwesterly winds and ISM rains are dominated. The Hormoz Strait area thus is the boundary between the extratropical, winter rainfall domain, and

the tropical, summer monsoon rainfall domain. However, it is suggested that, due to orbitally-driven insolation forcing, during the early-mid Holocene, a more northern position of ITCZ caused monsoon-induced summer precipitation in the study area (Fleitmann et al. 2007). Many Holocene paleoclimate records suggest that environmental changes triggered a range of cultural responses, from demise to reorganization, to the expansion of ancient societies in southern Iran. According to these studies, Bronze Age civilizations along rivers in southern Iran such as Tape Yahya and Konar Sandal (Majidzadeh 2003; Potts et al. 2001) along the Halil River, Shahdad (Salvatori and Vidale 1982) beside the Shahdad River and Shahr-e Sukhteh (Tosi 1983) ashore Hirmand River flourished around 7 - 4 kyr BP due to mid-Holocene ISM-induced climatic optimum. After this period, the southward migration of ITCZ caused relatively stronger ISM-dominated rainfall gradually replaced by the weaker Mediterranean winter precipitations, and consequently, the demise of the above civilizations. This can be attributed to the precessional shift of perihelion from September in the middle Holocene to January today over the last 5000 years which caused the reduction in insolation during the summer season in the Northern Hemisphere. At the same time, insolation increased during winter on almost the whole Earth (Rimbu et al. 2004). Therefore, the SH is a remarkable environment to assess the orbitally-induced temperature and wind regime changes as well as the proportions of various atmospheric systems affecting the paleoceanography and hydro-climatic regime of the area.

2.1.2. PG circulation and water exchange through the SH

As a semi-enclosed continental shelf sea, the PG exhibits many results of SST and wind intensity changes, as well as constricted water exchange with the open ocean. The region comprised of the PG, SH, and the Gulf of Oman is submitted to a strong solar heat flux, which leads to substantial evaporation (approximately 1.5 m yr^{-1}). In the PG basin, from April to July a barotropic cyclonic gyre governs the general circulation. Due to the winter cooling, and under influence of wind forcing (leading to a decrease in stratification), this pattern breaks down into smaller features (Pous et al. 2015). Evaporation (proportional to the ocean-atmosphere temperature difference and the wind velocity) leads to the formation of a warm and salty (dense) water mass in the PG called PGDW (Persian Gulf Deep Water) which is one of the most saline water masses in the world ocean (Reynolds, 1993). PGDW is formed at two locations including: a) the northwestern part of the PG, along the Kuwait and the Saudi Arabia shallow coasts, and b) over the southern banks (Arabian shallow shelf) (Fig. 1b); at both places,

the deep water masses are formed during fall and winter (Yao and Johns 2010; Lorenz et al. 2020). Due to their different distance to the SH, the first and the second water masses reach the SH during summer-early fall and late winter-spring respectively. A permanent southeastward deep current advects the dense water from the northwest towards the SH year-round, while dense water formed in the southern banks can flow to the SH by November to April. However, some minor sources of PGDW are located in central parts of the PG basin all year round (Pous et al. 2015). The maximum transport occurs in July with a value of 150.000 $m^3 s^{-1}$, while the minimum transport (70.000 $m^3 s^{-1}$) occurs in January (Johns et al. 2003). The PGDW is flushed out of the PG through the SH (Johns et al. 2003) and then stabilizes at depths of 250-350 m in the Gulf of Oman. It spreads first along the Omani coast (Bower et al. 2000) and forms coastal undercurrents.

The PGDW leaving the PG near the bottom of the SH is compensated by the surface inflow of Indian Ocean Surface Water (IOSW) (Johns et al. 2003, Yao and Johns 2010). All year round, an inflow of low-salinity IOSW enters the PG, on the Iranian side of the SH. Then, under the influence of the Coriolis force, it is deflected to the North (along the Iranian coast) and it forms a basin-wide cyclonic circulation in the southern PG (Fig. 1b). It is worth mentioning that at the SH, the IOSW bifurcates and that a large volume of water enters the PG south of the Qeshm Island, while the rest enters the PG through the Khuran Channel, a tidal channel located north of the Qeshm Island (Khosravi et al. 2018).

The inter-annual variability of the PG average salinity is significant, and it dominates the seasonal variability. These long-term variations are more related to the water exchange at SH than to atmospheric fluxes. These water exchanges at the strait play an essential role in the PG salt budget. The inter-annual variations of the circulation due to the variations in (E-P) significantly impact the net transport at SH. This circulation is driven by various mechanisms (density gradients and wind stress), and by their nonlinear interactions (Pous et al. 2015).

The IOSW inflow exhibits a significant seasonal variability. The volume flux of IOSW at SH is 7250 $km^3 yr^{-1}$ (Sheppard et al. 2010) and it is weaker (about 10 cm/sec) in spring and autumn and stronger (about 20 cm/sec) in summer (Hunter 1986) suggesting an increased transport of IOSW to the northwestern PG. The salinity of the outflow has a mean value of 39.3 psu with considerable intra-seasonal variability (ranging from 39.5 to 40.8 psu). The PGDW volume flux at SH is 6620 $km^3 yr^{-1}$ (Shepard et al. 2010).

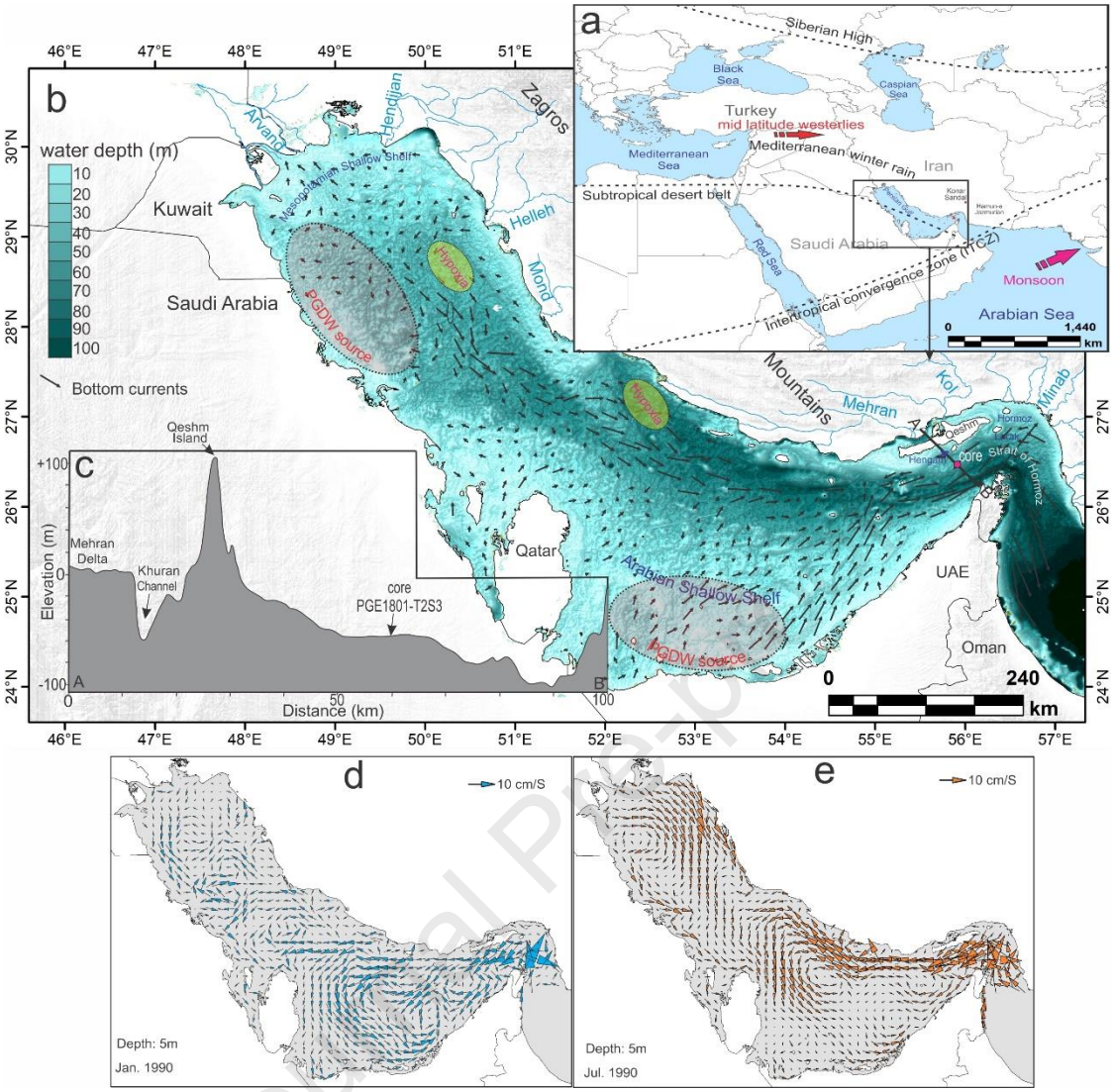


Fig. 1. a) General map of the Middle East containing the modern climatic setting including the boundary between the Mediterranean winter rain domain and the subtropical desert belt (after Arz et al. 2003), the position of the ITCZ (Regard et al. 1997) and Siberian High (Mayewski et al. 1997). b) The PG and SH and dominant bottom currents (Pous et al. 2015). c) Depth transect (A-B) perpendicular to the SH axis showing the coring location. d) surface currents in winter and e) summer (Pous et al. 2015).

At the SH, the vertical structure of the flow is a two-layer exchange in winter; the surface inflow has a salinity lower than 38.5 psu in the northern part of the SH; the deep outflow has a temperature of about 24°C and salinity of 40.5 psu. The deep outflow and the surface inflow speeds in winter are about 10 cm/s. In summer and fall, in addition to the upper inflow of IOSW and of the deep outflow, the warm and salty waters from the northwestern and southern banks feed an outflow at intermediate depths (between 10 and 40 m) in the southern part of the strait. The temperature and salinity of the outflow water are < 27 °C and >40.5 psu respectively, with a maximum velocity of 20 cm/s (Johns et al. 2003).

2.2. Coring and relevant analyses

The data of this study are the result of analyzing a 133 cm long sediment core PGE1801-T2S3 (hereafter called T2S3) retrieved during the Persian Gulf Explorer (PGE) cruise in January 2018 (PGE1801). The core was taken at the depth of 56 m west of Strait of Hormoz (15 km, south of Hengām Island (lat: 26.464833, long: 55.914841)) by a gravity corer with a 5 cm diameter (Fig. 1). Although the core was retrieved from the edge of the deep central channel of the SH, however, it lies below the depth of the PGDW outflow domain, at least during summer (Azizpour et al. 2014). Dissolved Oxygen (DO) and salinity of water samples taken from the surface, 5 m depth and bottom in this cruise (winter 2018) and cruise PGE1803 (summer 2018) were measured by a Hach multimeter. In the laboratory, an MS2C Bartington magnetic susceptibility meter was used for whole-core Magnetic Susceptibility (MS) measurements at 1 cm increments. Then, the core was cut along the longitudinal axis and one half-core used for reconstruction of the SST of the PG (Safarkhani et al. 2021) and another half-core used for this study. Initially, the preliminary studies including the imaging and the accurate description of sedimentological observations and sedimentary structures were done. Fifty-three subsamples were taken at 2.5 cm intervals (each sample covers ~35-165 years depending on the sample depth (Fig. 2)). 10 cm^3 from wet sediment was taken using the syringe technique to determine physical properties of sediment including water content, porosity and wet bulk density (Mudroch et al. 1997). Total Organic Matter and carbonate per cent were measured using the loss-of-ignition (450 °C, 5 h) and acid dissolution methods (hydrochloric, 1N), respectively (Heiri et al. 2001; Mudroch et al. 1997). Sand and mud fractions were separated by wet sieving (using 63 μm sieving). A FRITSCH laser particle sizer was used to separate silt and clay fractions as well (Konert and Vandenberghe, 1997). >250 μm fraction from a 10 cm^3 sediment samples was used for counting relict particles under Nikon stereomicroscope (Sarnthein 1971). Finally, the >63 μm fraction was used to obtain census data of benthic foraminiferal assemblages. The foraminiferal taxa were identified by Haynes (1981) and Loeblich and Tappan (1988) textbooks and previous studies of the area (Amao et al. 2018; Saidova 2010). At least 300 individuals were counted to determine the relative abundance of species to characterize an assemblage (Murray, 2006). Benthic foraminiferal accumulation rate (BFAR)

(number of specimens/cm^2 10 yr^{-1}) were measure based on Herguera (1992). All frequency and abundance of benthic foraminifers are reported per 10 cm^3 of sediment.

2.3. Radiocarbon dating

After evaluating the physical properties of the core sediments (especially MS), three sediment samples were taken from depths of 50, 90 and 120 cm (Table 1, Fig. 2), where significant changes happen (Fig. 3). As the organic remains contained in bulk sediments may originate from numerous sources of different ^{14}C ages, thus yielding inaccurate ages, we collected benthic foraminiferal tests (*Ammonia beccarii*; Linnaeus, 1758) to obtain more precise dating results (Olsen et al. 2017). *A. beccarii* tests with the size range of 300 to 500 µm were picked and sent to the Poznan laboratory to determine the age by AMS radiocarbon method and calibrated using Marine20 (Reimer et al. 2020) regarding the value proposed as the reservoir effect for the PG and the Arabian Sea ($\Delta R = 190 \pm 25$; Southon et al. 2002). The ages were reported based on the mean probability of error 2σ (Table 1). Age-depth relationship of core T2S3 produced by CLAM software (Blaauw 2010). All ages mentioned in this study are reported as the year before the present time (cal yr BP) and thousands of years before the present time (cal kyr BP).

Table 1. Radiocarbon age report for three benthic foraminifera samples from the core T2S3. ^{14}C ages were calibrated based on Marine 13 calibration dataset.

Sample number	Laboratory number	Sample material	Number of tests	Sample weight (g)	Depth (cm)	Age (2σ ±) (yr BP)	Calibrated age range (cal yr BP)
TS-50	Poz-107160	*A. beccarii*	278	0.049	50	2120±30	1370-1580
TS-90	Poz-107161	*A. beccarii*	183	0.039	90	2595±30	1921-2144
TS-120	Poz-107162	*A. beccarii*	251	0.058	120	4420±30	4195-4439

3. Results

3.1. Age-depth model

Figure 2 shows the age-depth diagram of the core based on three age-determined samples considering the zero time for surface sediments. In this way, the line of changes in the core age

was plotted between four horizons of zero, 50, 90 and 120 cm. Since the characteristics of sediment material of deeper than 120 cm (the lowest age-determined sample) do not show significant changes, the age-depth diagram in the end part is extended to the end (bottom 13 cm) without changing the slope. As such, the age determination diagram is plotted assuming that the sedimentation rate (SR) is uniform between the age-determined horizons (Figure 2).

The highest SR (0.72 mm yr^{-1}) is observed in the middle parts of the core (depth 50-90 cm), while the lower depths represent the lowest (0.15 mm yr^{-1}). With an SR of 0.34 mm yr^{-1}, the topmost section lies in between. The overall SR of the core T2S3 is in agreement with the findings of Al-Ghadban et al. (1998) in the SH.

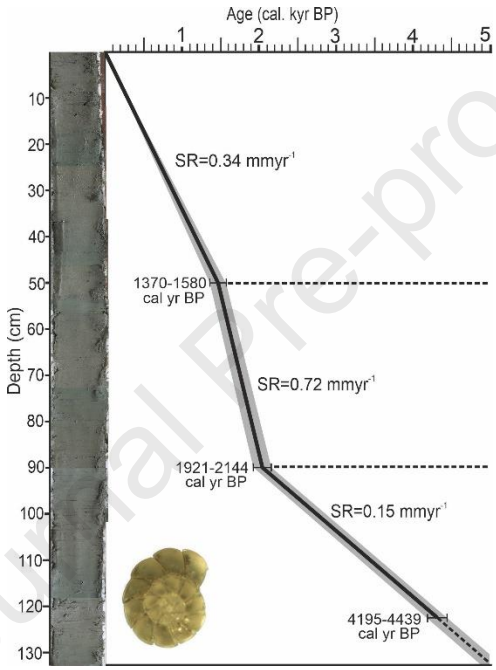


Figure2. Age-depth diagram of core T2S3 from three age-determined samples. The Grey bars show 95% confidence intervals. The image of the age-determined foraminifera (*A. beccarii*) is shown at the bottom of the figure.

3.2. Dissolved oxygen and salinity of the water column

The characteristics of the water column at the SH shows that, during summer when the water layers are distinctly formed and PGDW is strengthened, DO differences between the surface (6.44 mg/l) and bottom (3.25 mg/l) are relatively high. However, at the same time, hypoxic conditions (DO < 1 mg/l) prevail at some areas deeper than 50 m in the central and western basins of the PG (Fig. 1d) which are not located on the path of PGDW (Saleh et al. in press). PGDW salinity at this time is 40.8 psu as well. In winter, DO concentrations at the surface,

depth 25 m and bottom (depth 56 m) are 5.61, 5.43 and 4.79 mg/l respectively. Bottom salinity during winter is 39.0 psu which is 1.8 psu lower than that of summer. This slight difference between the surface and bottom is attributed to the vertical mixing. This shows that the PGDW has a fundamental role to provide DO at the bottom of the SH, especially during summer when the situation in other deep areas of the PG and SH is unfavourable for benthic communities.

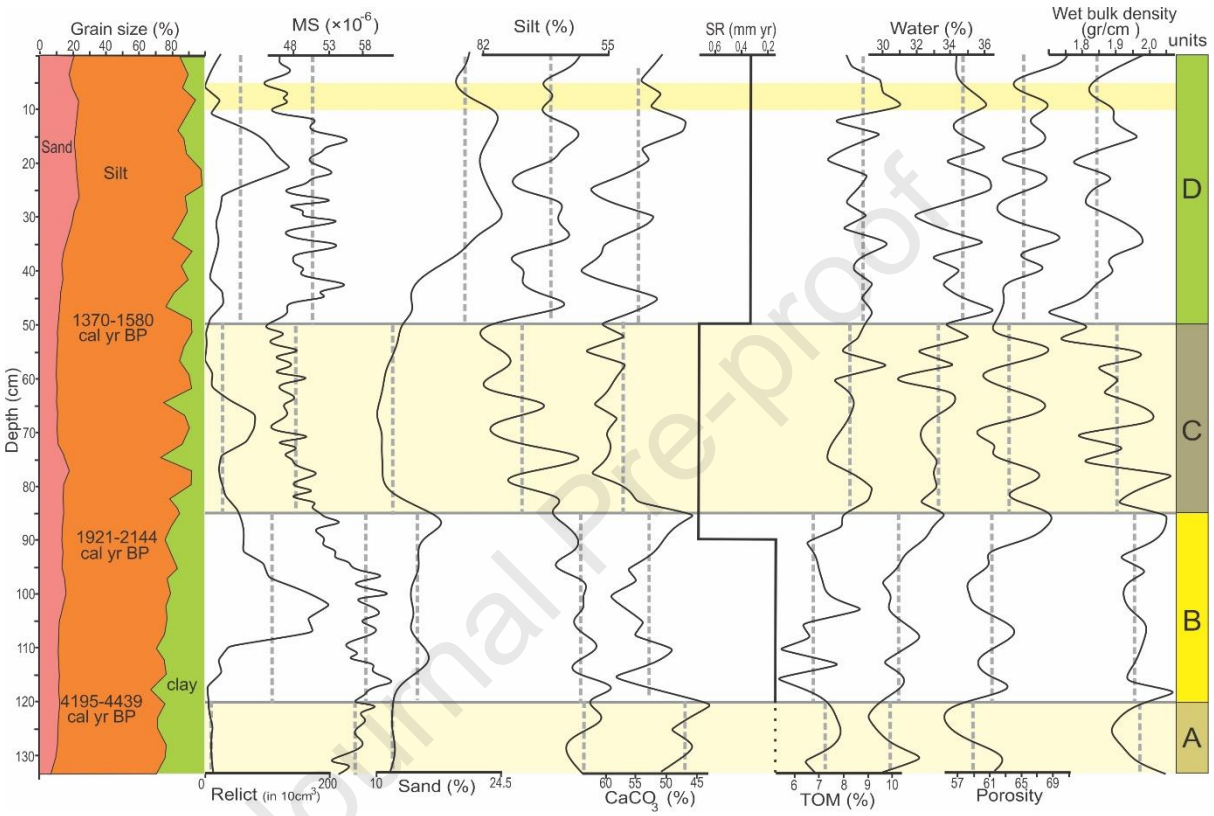


Fig. 3. Variations in sedimentological and geochemical characteristics in core T2S3. Graphs range between minimum and maximum values. Vertical dashed lines show the average values in units.

3.3. Sedimentological characteristics

The lithology of the core T2S3 mostly consists of pale olive (5Y 6/3) sandy silt units. Only the sediments of the bottommost sample (below 130 cm), due to falling sand content below 10%, are silt. Generally, sedimentological proxies can be classified into two groups. The first one varies somewhat steadily with depth and shows an increasing or decreasing trend upward. These parameters following post-depositional influences (i.e. compaction and degradation) include TOM, water content, porosity and wet bulk density. Due to the sediment compaction, water content and porosity of core sediments increase upward, while wet bulk density shows a reverse trend (Fig. 3, Table 2). TOM variation has a decreasing downward trend. The members

of the second group show more intricate variations likely due to the paleoenvironmental changes during the sedimentation. The variation trend of relict particles, MS and sand content show a slightly positive correlation. On the other hand, SR, silt content and calcium carbonate per cent variations are positively correlated. Moreover, the two above groups of proxies oscillate conversely.

The relict grains are a mixture of various components including mostly black ooids, faecal pellets, mollusc shell fragments, bryozoa, foraminifera as well as corals. Furthermore, light coloured terrigenous particles are also observed (Fig. 4) which are embedded in an aragonite mud matrix. Sarthein (1972) defined the palaeoenvironment of this community as a transformation of successive intertidal carbonate areas into deep water areas. He also suggests that the processes of black colouring and glauconization of grains, and the weathering on the surface of the skeletal remains most likely took place in the early, shallow water stage.

Altogether, based on basic sedimentological data, MS as well as foraminiferal assemblages, we have recognized four units, A, B, C and D (Fig. 3). According to Fig. 3, some abrupt changes in MS values and grain size distribution can be distinguished, which could be related to changes in sediment transportation/deposition conditions.

Table. 2. Variations in sedimentological and geochemical characteristics in four units of core T2S3.

	Unit A 120-133 cm 4320-5000 cal yr BP		Unit B 85-120 cm 1980-4320 cal yr BP		Unit C 50-85 cm 1470-1980 cal yr BP		Unit D 0-50 cm 0-1470 cal yr BP		Entire the core	
	Range	Ave.	Range	Ave.	Range	Ave.	Range	Ave.	Range	Ave.
Sand (%)	8-13	11	12-18	15	10-16	11	13-24	19	8-24	15
Silt (%)	60-67	63	56-68	62	59-82	74	62-79	69	56-82	69
Clay (%)	22-29	26	16-32	23	7-26	14	2-23	12	2-32	17
MS ($\times 10^{-5}$ SI)	5.6-5.6	5.6	5.2-6.2	5.7	4.4-5.6	4.8	4.4-5.4	5.0	4.4-6.2	5.2
Relict no (in 10 cm^3)	11-18	15	9-210	101	5-87	38	5-145	45	5-210	52
CaCO3 (%)	43-51	47	49-59	54	50-63	58	50-64	56	43-64	55
TOM (%)	6.4-7.9	7.3	5.3-8.6	6.8	7.4-9.7	8.3	7.3-10.4	8.8	5.3-10.4	8.0
Porosity	55-63	59	58-66	61	57-70	64	60-71	65	55-71	63
Wet bulk density (gr/cm^3)	1.9-2.1	2.0	1.9-2.0	2.0	1.7-2.1	1.9	1.7-2.0	1.8	1.7-2.1	1.9

Unit A: This relatively thin basal unit represents the lowest sand (8-13 %), silt (60-67 %) and calcium carbonate (43-51 %) content of the core with an upward increasing trend. The number of relict particles is lower than that of other units, too. Conversely, the MS values are higher than in other units except for B.



Fig. 4. Digital image of some relict particles including terrigenous (a-h), ooids/pellets (i-j), benthic foraminifera (k-o) as well as bivalve (p) and crustacean shells (q). some of the terrigenous particles are embedded in an aragonite cement (b).

Unit B: MS an increasing upward trend in the former unit is continued to the base of unit B to reach the maximum values (5.2 – 6.2 $\times 10^{-5}$ SI) in this unit. Sand and $CaCO_3$ content increase by 15-30 % in this horizon as well. However, the most dramatic increase happens in relict particles. The number of these grains in this unit is 7 times more than that of unit A. On the other hand, silt content remains relatively unchanged and, together with unit A, are lowest in the core. These low values coincide with the lowest sedimentation rate (0.15 mm yr^{-1}).

Unit C: An abrupt decrease in the number of relict particles (2.6 times) separates this 40 cm long unit from the above and below ones. This decline correlates with decreasing sand content and MS values (16 and 14 % respectively) with a lower magnitude. Instead, silt (mean: 74%) and calcium carbonate (mean: 58%) content co-increase with the sedimentation rate (0.72 mm yr^{-1}) and attain their highest values in the core.

Unit D: This unit is characterized by a re-increasing number of relict particles, MS values and sand content. The magnitude of these variations for relicts and MS (18 and 4 %) is lesser than

Journal Pre-proof

that of sand content (42%). The mentioned increases correlate well with the decreasing silt and calcium carbonate contents (7 and 3 % respectively) as well as the sedimentation rate from 0.72 to 0.34 mm yr^{-1}).

3.4. Foraminiferal assemblages

Seventy different foraminiferal species are recognized, of which 35 are Rotaliida, 21 are Miliolida, 6 are Textulariida, 6 are Legenida, 2 are Lituolida and one is Astrorhizida (A1). The variation in the number of specimens and percentages of benthic foraminiferal taxa are illustrated in figure 5. The assemblages are dominated by hyaline taxa (60%), while porcelaneous (25%) and agglutinated (15%) are placed in the second and third order. Ten most abundant genera are *Bolivina* (26%), *Quinqueloculina* (21%), *Ammonia* (13%), *Nonion* (10%), *Trochammina* (9%), *Cassidulina* (4%), *Bulimina* (4%), *Spiroloculina* (2%), *Textularia* (1%), *Asterorotalia* (1%), *Hanzawaia* (1%) and *Fissurina* (1%). Other subsidiary taxa such as *Triloculina*, *Marsipella*, *Elphidium*, *Cancris*, *Cribroelphidium*, *Sigmilopsis*, *Cibicides*, *Lagena*, *Challengerella*, *Rosalina*, *Cornuspira*, *Hyalinea*, *Fursenkoina* comprises <1 - 0.1% of the foraminiferal assemblage. This assemblage is relatively invariant in all of the units. The foraminiferal fauna shows a shelf edge to upper slope association characteristics (Saidova 2010, Murray, 2006).

As a general trend, the species richness, number of specimens and fisher alpha index (Fisher et al. 1943) of units B and D are much higher than those in units A and C. Mean species richness and number of individuals in the core are 30 and 5200 respectively. Mean species richness in units A and C are 7 - 17% less and in B and C units are 10-17% more than that of the whole core. Unit B represents the highest number of individuals (6670) and units D (5150), A (4850) and C (4150) lie at the next orders. Fisher Alpha index also follows the above arrangement. The frequency of nearly all taxa also follows the above trend. Large specimens (>250 µm) mostly include *A. beccarii* (45%), *Challengeralla bradyi* (25%) and *Asterorotalia milletti* (20%). *Triloculina tricarinata* and *Spiroloculina depressa* comprise a minor fraction. The number of these specimens is by far highest in unit D (74 - 450; mean: 264), and unit B (53 – 165; mean: 104) lies in second place. The average of this value in two other units is less than 100. The relative average of epifaunal to infaunal taxa in the whole core is 0.82 and shows an increase in units B (0.79) and D (0.96) compared with units A (0.68) and C (0.74).

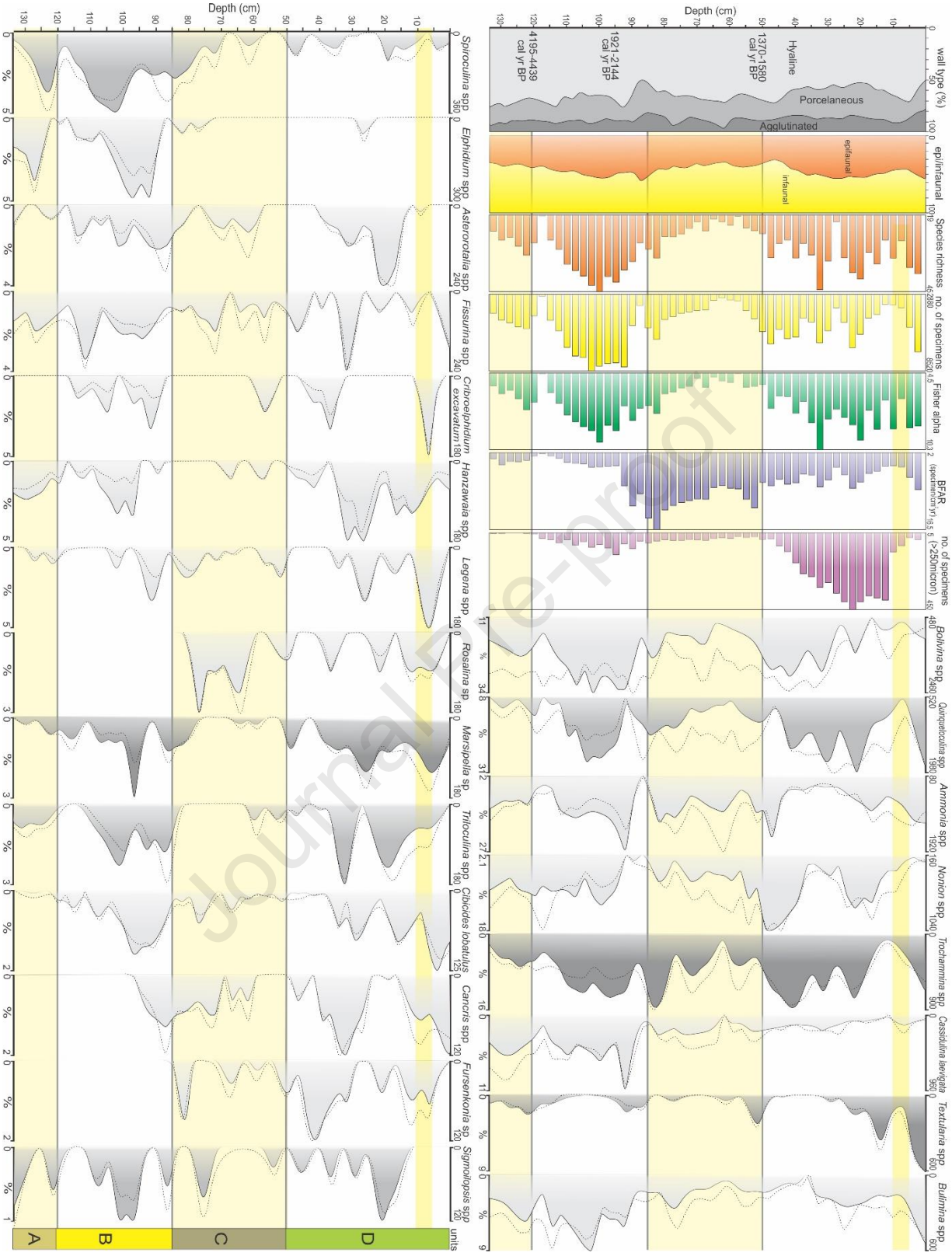


Fig. 4. Down-core variations in number (solid areas), and percentage (dashed lines) of foraminiferal taxa. Graphs range between minimum and maximum values along the core sediment. Very light, light and dark grey graphs represent hyaline, porcelaneous and agglutinated taxa respectively.

Down-core variation in the frequency of the foraminifera indicates that most of them are enriched in units B and D. However, these variations in some genera such as *Quinqueloculina*, *Marsipella*, *Triloculina* and *Cibicides* show a higher magnitude while in some others (*Bolivina*, *Ammonia*, *Nonion*, *Trochammina*, *Bulimina* and *Fissurina*) have lower intensity. *Cassidulina*, *Spiroloculina* and *Elphidium* decrease upward, while *Textularia* and *Fursenkoina* represent a reverse trend. Altogether, the enrichment of individuals in both units B and D correlates well with the decreasing sedimentation rate. As is demonstrated in Figure 4, BFAR in units D, and especially B, is lower than that of unit C. Indeed, in these units (unlike unit C) the specimens are relatively less diluted by sedimentation. Therefore, to eliminate the effect of dilution by sediment deposition, the BFAR and accumulation rate for all foraminiferal genera were calculated. To compare the BFAR in two distinct sedimentary environments including 1) units A and C with relatively low MS, sand content, relict particle, SR and high silt and calcium carbonate content and 2) units B and D with a completely opposing trend, we calculated the accumulation rate percentage for all foraminifera in units B and D ($\%AR_{BD}$) (Table 3).

$$\%AR_{BD} = [(AR_B + AR_D) / (AR_A + AR_B + AR_C + AR_D)] \times 100$$

Where $\%AR_{BD}$ is the percentage of accumulation rate for specific foraminifera in units B and D, and AR_A, AR_B, AR_C and AR_D are accumulation rate for the same foraminifera in units A, B, C and D respectively.

Table 3 indicate that the highest $\%AR_{BD}$ (>50) mostly belongs to the clinging epifaunal foraminifera attached above the ambient hard substrate or coarse sediment surface in a high-energy environment (*Hanzawaia*, *Cibicides Marsipella*, *Hyalinea*, *Textularia*) (Murray 2006, Schönfeld 2002a). By moving toward the lower values (50 – 43%) free epifaunal taxa living on a finer substrate (*Asterorotalia*, *Quinqueloculina*, *Trichammina*, *Cornuspira* and *Cancris*) prevail. The benthic foraminifera with the lowest $\%AR_{BD}$ values is dominated by infaunal free foraminifera living in muddy sediments. These taxa involve *Bolivina*, *Ammonia*, *Nonion*, *Cassidulina*, *Oolina* and *Fissurina*.

Table. 3. Accumulation rate of benthic foraminifera in four units of the core T2S3 and their ecological characteristics (Murray 2006). The genera are arranged based on $\%AR_{BD}$ values

Genera	Mean AR				$\%AR_{BD}$	Mode of life*	Substrate
	Unit A	Unit B	Unit C	Unit D			
Hanzawaia	0.40	0.29	0.27	1.09	**67.0**	E, C	H

Journal Pre-proof

Challengerella	0.00	0.00	0.10	0.20	**66.9**	E, F	,H
Cibicides	0.00	0.31	0.41	0.50	**66.0**	E, C	H, HE
Marsipella	0.09	0.27	0.51	0.86	**65.5**	E, C	H, HE
Cribroelphidium	0.00	0.24	0.39	0.40	**62.0**	I, F	fS/cS
Hyalinea	0.00	0.03	0.20	0.27	**60.2**	E, F	cS
Triloculina	0.26	0.33	0.62	0.78	**55.6**	E, F/C	cS
Spirophtalmidium	0.14	0.17	0.00	0.00	**55.6**	E, F/C	cS
Textularia	0.36	0.14	0.91	1.43	**55.3**	E, F/C	cS
Fursenkoina	0.00	0.00	0.40	0.50	**55.1**	I, F	fS
Bulimina	1.59	2.17	3.61	2.47	**47.2**	I, F	fS/cS
Sigmoilopsis	0.22	0.22	0.44	0.33	**46.0**	E, F/C	cS
Asterorotalia	0.13	0.39	1.35	0.82	**45.0**	E, F	cS
quinqueloculina	3.59	6.49	24.12	16.05	**44.9**	E, F/C	fS/cS
Trochammina	1.70	3.15	10.82	6.49	**43.5**	E/I, F	fS/cS
Cornuspira	0.10	0.01	0.12	0.16	**43.0**	E, F	fS/cS
Lagena	0.09	0.11	0.79	0.55	**43.0**	I, F	fS/cS
Elphidium	0.70	0.81	0.47	0.06	**42.7**	E/I, F	fS/cS
Cancris	0.00	0.05	0.98	0.67	**42.5**	E, F	fS/cS
Nonion	3.02	3.25	10.68	6.77	**42.2**	I, F	fS
Bolivina	7.74	10.56	28.91	15.70	**41.7**	I, F	fS
Fissurina	0.50	0.63	1.43	0.74	**41.3**	I, F	fS
Ammonia	3.48	4.56	16.56	7.32	**37.2**	I, F	fS/cS
Spiroloculina	0.86	1.16	2.14	0.57	**36.6**	E, F/C	fS/cS
Cassidulina	2.52	2.49	4.57	1.28	**34.7**	I, F	fS
Oolina	0.00	0.04	0.22	0.00	**14.7**	I, F	fS

E: epifaunal; I: infaunal; C: clinging; F: free; H: hard substrate; HE: high-energy conditions; fS: fine sediments; cS: coarse sediments; AR: accumulation rate (no. of specimens/cm^2 10 yr^{-1}); AR_{BD} : (AR in unit B + AR in unit D) / (AR in whole core) × 100.

4. Discussion

In this section, the variation of the PGDW strength is reconstructed using faunal and non-faunal proxies, and then, its possible link with the paleoenvironment of SW Asia is evaluated.

4.1. Application of faunal and non-faunal indicators to reconstruct PGDW variations

4.1.1. Non-faunal indicators

The PG shows a striking and unique sedimentation pattern which can be employed to correlate with the hydrodynamic conditions that control sediment transport. The Iranian part is the region of extensive terrigenous sediment input from occasional violent flash floods building up a complex coastal plain and covering the northern half of the PG by silt-sized sediments (Baltzer and Purser 1990; Purser and Seibold 1973). The Arabian shallow shelf, on the contrary, is the site of intensive and rapid deposition of carbonate sediments which are traceable in bottom

sediments of the PG, commonly as sand and pebble fractions (Evans, 1973). These two contrasting sedimentary basins with their specific ecological characteristics come together in the narrow channel of SH. Besides, these modern sediments are mixed with a significant amount of relict sediments, left on the shelf when it was exposed during the last glaciation (Purser and Seibold 1973). Sediment texture and composition becomes more complicated when the influence of density-driven PGDW is considered (Reynolds 1993).

Using grain-size and pteropod distribution in 12 sediment cores retrieved from the northern half of the PG, Diester-Haass (1973) suggested that the most reliable indicator of the Holocene climate change are terrigenous materials carried into the PG by rivers. During increased terrigenous supply, the silt-size layer was dominated, while the lesser supply of terrigenous material resulted in the deposition of a coarse-grained layer. Furthermore, the coastal area of mainland and the Qeshm Island is mainly composed of easily erodible Eocene to Miocene limestone rocks such as calcareous sandstone and marls (Molinaro et al. 2004) providing detrital carbonates as a significant fraction of terrigenous sediments (Hamzeh and Farahi Ghasr-Aboonasr 2020; Baltzer and Purser 1990). Volcano-sedimentary units comprise a negligible amount of terrigenous sediments. Hence, unit C in which a co-increase in the amount of silt and carbonate (which is correlated with the SR) takes place corresponds to a relatively humid period with high terrigenous input. Some parts of the PG receiving little recent sedimentation or experiencing high energy bottom currents are characterized by bottom samples containing considerable quantities of skeletal and non-skeletal relict sediments (Diester-Haass 1973). The relict grains, observed in deeper parts of the PG, have a shallow water origin with radiocarbon ages of 7000-13000 years (Sarnthein 1972). A decreasing percentage of sand fraction and relict particles which reflects the degree of dilution by terrigenous materials, together with the decline in the MS values, also confirms the above statement. This situation is observed in unit A with a lesser magnitude as well. Safarkhani et al. (2021) also suggested that these relatively humid periods are well correlated with declining SST at the PG. All the above parameters oscillate conversely in both other units (B and D) indicating a quite different environmental condition. These dry units are contemporaneous to the periods of SST elevation at the PG. During the periods corresponding to units B and D, increasing 1-2°C in SST means increasing heat flux and freshwater loss in the PG, which are the main drivers of the dense water formation and its propagation to the SH. Strengthening the PGDW leads to removing fine sediments and remaining coarser ones as well as the reduction in SR in the mentioned units. However, as the coring site is located at the border, instead of the bottom of the main outflowing channel, the PGDW traces on sediments are modified.

Journal Pre-proof

460

461 **4.1.2. Faunal indicators**

462 There have been few studies about the ecology of foraminifera in the PG (Murray 1965, 1966,
463 1970; Basson and Murray 1995; Parker and Gischler 2015), especially at the Iranian sector
464 (Haake 1970, 1975; Nabavi et al. 2014); these studies are patchy and none of them concerned
465 the SH. Some more comprehensive studies (i.e., Amao et al. 2018; Saidova 2010; Cherif et al.
466 1997) have dealt with the nearly entire PG. However, two of the latter covered the SH. The
467 assessed foraminiferal fauna belongs to the continental shelf which is also influenced by the
468 upper slope association. These taxa are very similar to assemblages previously described from
469 the SH and adjacent areas with relatively deeper, warmer, and more oxygenated conditions
470 comparing to other parts of the PG (Amao et al. 2018; Saidova 2010).

471 The observation that a specific assemblage of benthic foraminifera occurs in areas with
472 elevated current velocities (Schönfeld, 2002a, 2002b, 1997) has led to the tentative
473 development of a proxy for bottom current velocity. Investigating down-core variation of
474 benthic foraminifera as the precise indicators of the bottom current strength can provide us
475 with valuable information about bottom paleo-current variations. Coarse grains flooring high-
476 energy areas provide a substrate for attachment of some groups of foraminifera (Kucera 2007;
477 Murray 2006). In these bottom environments, epifaunal foraminifera are relatively abundant
478 and live preferentially on elevated substrates such as coarse shell debris, sponges, crinoids,
479 hydroids, tube worms, or living arborescent benthic foraminifera (e.g., *Rhabdammina* spp.), as
480 well as large terrigenous particles (Kucera 2007; Sen Gupta et al. 2006). These specialized
481 epibenthic foraminifers can also catch suspended organic matter particles (Murray 2006).

482 The number of benthic foraminifera in units A and C is, by far, smaller than that of
483 units B and D. However, this bareness (particularly in unit C) is due to the dilution by high
484 sedimentation rate of terrigenous material. Low BFAR in units B and D may be due to
485 prevailing unfavourable conditions in the corresponding periods. As studies show, high energy
486 bottom currents provide hostile environments, making the number of individuals and species
487 diversity low to moderate (Murray 2006). The increasing proportion of epifaunal foraminifera
488 which is mostly suspension feeder (such as *Hanzawaia*, *Cibicides*, *Marsipella*, *Hyalinea*,
489 *Triloculina* and *textularia*) in Units B and D may be attributed to the domination of high-
490 velocity currents in the corresponding periods. Schönfeld (2002a, 1997) also suggests these
491 assemblages having a high proportion of attached forms are indicative of high-energy shelf
492 areas. The results showed assemblage of sessile epifaunal and/or epibenthic suspension feeders

493 on the Spanish continental margin, influenced by high energy bottom currents related to the
494 Mediterranean Outflow Water. He also indicated a linear correlation between the percentage
495 of typical taxa for elevated microhabitats and bottom water current velocity and used this
496 relation to reconstruct the Holocene history of bottom current velocity at the southern
497 Portuguese margin (Gulf of Cadiz). *Quinqueloculina*, *Asterorotalia*, *Cancris* and
498 *Cribroelphidium excavatum* which are commonly observed in sandy substrates (moderate
499 energy) (Murray 2006) are also present as subsidiary taxa in these two high energy units.
500 Saidova (2010) indicated that these taxa (particularly *Quinqueloculina*, *Asterorotalia*, and
501 *Textularia*) show a preference for areas with minimal river discharge in the PG. These units
502 (particularly unit D) also bear the highest percentage of robust tests (>250 μm) (Schönfeld,
503 1997). It is a matter of observation that tests in high-energy environments are thicker-walled
504 and more robust so that they can control their buoyancy. These taxa are highly dependent on
505 the dissolved oxygen and remain of microalgae (phytodetritus) brought by PGDW (Saleh et al.
506 in press). Such a food source of high quality has been observed at 4000 m depth in the Arabian
507 Sea (Pfannkuche et al. 2000). Amao et al. (2018) concluded that the abundance of most of the
508 mentioned epifaunal taxa particularly *Asterorotalia dentata* and some *Elphidium* are positively
509 correlated with nutrient flux. On the other hand, the assemblages resembling Low-energy
510 muddy substrates including *Bolivina*, *Bulimina*, *Nonion*, *Ammonia* and *Cassidulina* (Murray
511 2006) are more abundant taxa in units A and C.
512

513 **4.2. Paleoceanography and paleoclimate of the SH**

514 The bottom sedimentation regime and the magnitude of density difference between the
515 PGDW and the water in the Gulf of Oman (which is the primary driver of water exchange
516 through the SH) are the main oceanographic phenomena of the SH being strongly under the
517 influence of surface temperature of land and sea (which lead to surface evaporation and then
518 dense water formation in the PG). Although IOSW temperature has a considerable role in SST
519 variations in the PG, however, the characteristics of the water masses formed in this landlocked
520 water body are mainly controlled by continental climate (Ghasemifar et al. 2020; Diester-Haass
521 1973). Consequently, the continental climate and IOSW temperatures are the main forcing
522 factor for water circulation (PGDW) and terrigenous sediment input in the SH.
523 Three main parameters of the Earth's orbit around the Sun controlling the seasonal
524 distribution of solar radiation at the top of the atmosphere are: 1) the eccentricity of the orbit
525 with the Sun in one of the two foci, 2) the time of the Earth's passage through its perihelion,

and 3) the tilt of its rotation axis (Milankovitch 1941). Over the last 5000 years, precession and obliquity cycles caused a shift of perihelion from late summer to early winter and a decrease in the tilt of the Earth's axis. The resulted radiative changes in the PG area caused a decrease in the boreal summer insolation and an increase in the boreal winter insolation (decreasing seasonality) (Fig. 6a). The seasonally averaged model results of Lorenz et al. (2006) imply that winter warming slightly exceeded the summer cooling in the area, resulting in moderate warming. Present-day warmer tropics (below 30° N) and colder extratropics (above 30° N) on the northern hemisphere compared to the middle Holocene climate is shown by many studies accordingly (Liu et al. 2003; Kim et al. 2004; Lorenz et al. 2006). The PG and the Oman Sea and their surrounding continents are in transitional zones of tropics and extratropics posing complex climate change trends in the area. In the boreal summer, the Arabian Peninsula and the Oman Sea experienced slight warming (<1°C), which is in line with the reduction of insolation by 15 W m^{-2}. Simultaneously, there is no Holocene temperature change or moderate cooling over the Iranian Plateau (<0.7°C) (Figure 6b). In the boreal winter, the Iranian Plateau, the Arabian Peninsula and the PG and the Oman Sea generally exhibit pronounced warming of 2.5 - 3°C. this gradual warming especially in winter (the season of PGDW formation in northwest and south of the PG) may be responsible for a general trend of increasing PGDW intensity since the mid-Holocene. Kim et al. (2004) also suggest that the Holocene weakening of the Arctic Oscillation/North Atlantic Oscillation (AO/NAO) pattern is associated with the tropical warming caused by the precession-related increasing boreal winter insolation. In boreal winter, a considerable mid-Holocene decrease evolved in sea level pressure difference between high latitudes (Icelandic low) and low latitudes including the continents bordering the PG (Azores high) (Lorenz et al. 2006). The climate models linked this decrease in east-west surface temperature difference with a Holocene weakening of the midlatitude atmospheric circulation, and therefore, reducing westerlies into the area. Altogether, the overall outcome of orbitally-driven solar insolation changes has been a gradual warming and weakening inflow of cold continental air masses primarily in winter (Felis et al. 2000) over the area since the last 5 millennia (Fig. 6a). However, as Mayewski et al. (2004) indicate, some short-term centennial-scale rapid climate change events disrupt this general warming trend. They suggest that solar variability superimposed on long-term changes in insolation seems to be the most likely responsible for these changes. The most notable instance is an abrupt SST increase centred at 3.8 cal kyr BP. A decline in ^{10}Be concentrations in the GISP2 ice core attributes this event to increasing solar output. This sudden SST elevation is traceable in the North Atlantic and western Mediterranean Sea (Fig. 6f and h).

Periods of high SST in the PG coincide with the increasing continental temperature and dryness over SW Asia and, in turn, a decline in terrigenous input to the PG and SH. The recent paleoclimate studies show, unlike the climate conditions during the early Holocene, ISM intensification during mid to late Holocene have harmed the hydroclimate regime of S Iran (Miller et al. 2016; Hamzeh and Farahi Ghasr-Aboonasr 2020). During the warm episodes, northward migration of the ITCZ and an intensification of the ISM system results in earlier spring maximum precipitation and a later autumn maximum precipitation (extending the length of the summer dry season), and therefore, increased drought (Djamali et al. 2010). In conclusion, paleotemperature changes in SW Asia (both continental and oceanic) can directly influence the variation of terrigenous input and PGDW of the SH.

4.2.1. Unit A: ~5000 – 4300 cal yr BP

Due to the lack of radiocarbon dating, the basement age of the core T2S3 is rather unclear. Indeed, its corresponding ~700-year period is the end of an SST decreasing trend started from the early-Holocene, and the beginning of an SST increase documented in the SH (Safarkhani et al. 2021), the Arabian Sea (Saher et al. 2007) and the North Atlantic Ocean (Kim et al. 2004) due to the reduction of summer solar insolation (Mayewski et al. 1997). During this period when the mean annual SST in the SH was 26.2°C (~1°C lower than that of today), the Arabian Sea salinity also decreased (Doose-Rolinski et al. 2001). A slight increase in terrigenous input is observed in this area which is contemporaneous to the optimum climate of the Iranian plateau and Near East (Bar-Matthews et al. 2003; Frumkin et al. 1991). Vaezi et al. (2018) showed a decrease in aeolian input together with an abrupt increase in rainfall between 5 and 4.7 cal kyr BP in the Hamun-e Jazmurian basin, about 140 km northeast of the SH. This optimal climate caused the flourishment of Bronze Age civilizations from Mesopotamia toward SE Iran and is attributed to the ISM-induced precipitations (Fleitmann et al. 2007; Cullen et al. 2000). As the proxies such as moderate increasing upward MS value, sand content and epifaunal communities as well as moderate decreasing upward in silt content show, a decline in SST of the PG and, in turn, eliminating SST contrast between PG and the Arabian Sea and reduction of evaporation rate caused PGDW strength to become moderate to low. Considering that this unit occurred just 2-3 thousand years after postglacial sea-level rise inundation, BFAR has been lower than that of subsequent units. Altogether, this period was wetter and colder than that of today and lower SST of the SH (due to colder continental climate and IOSW) led to decrease PGDW intensity (Fig. 7).

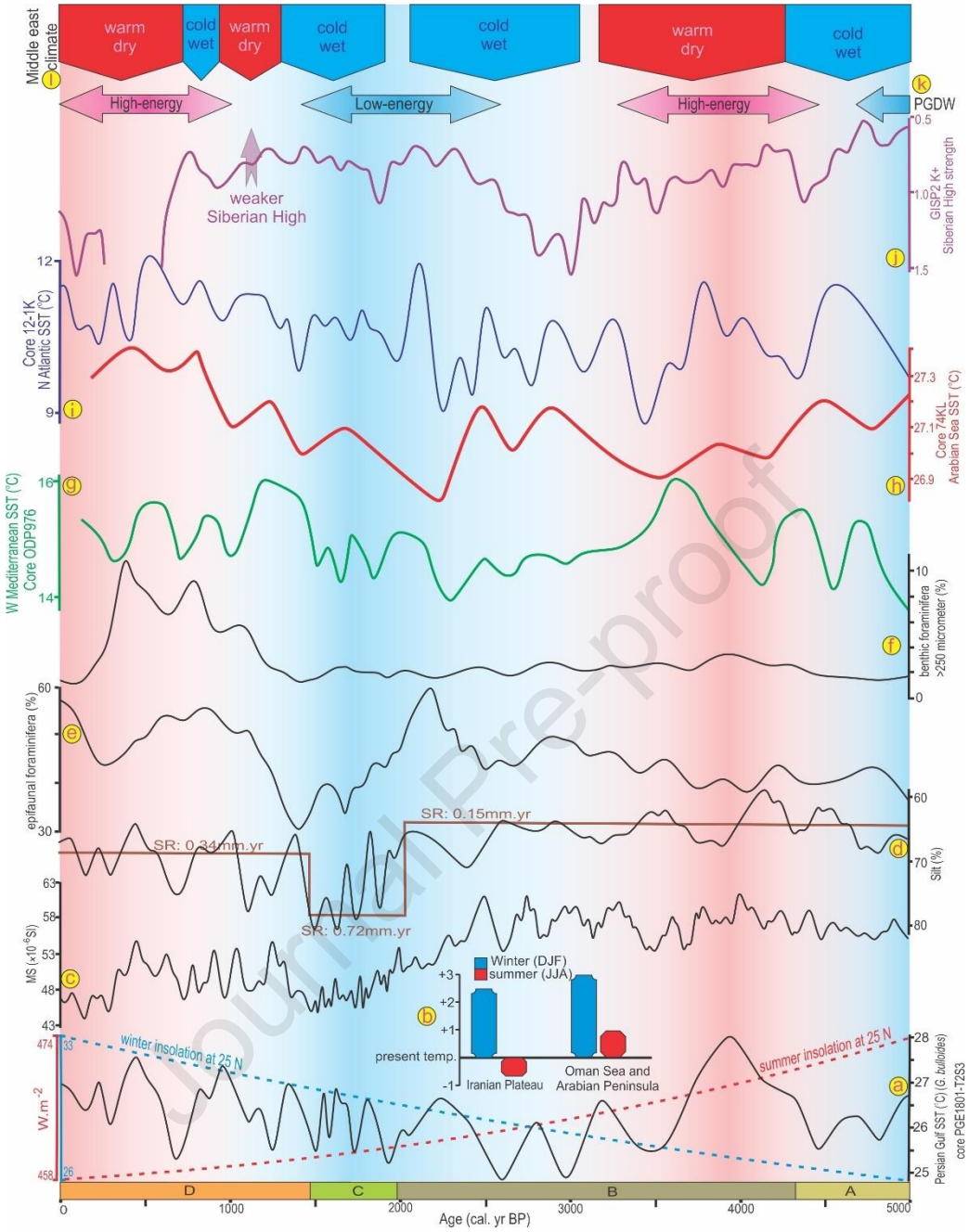


Fig. 6. Comparison of (a) Mg/Ca-derived SST in the SH measured in tests of *G. bulloides* from PGE1801-T2S3 sediment core (Safarkhani et al. 2021) as well as summer and winter insolation at 25 °N (Berger and Loutre 1991), (c) MS values with (d) silt content and sedimentation rate, (e) per cent of epifaunal foraminifera, and (f) per cent of >250 µm benthic foraminifera of the SH from PGE1801-T2S3 sediment core (this study). Furthermore, paleoclimate records from the surrounding regions, including (g) SST record from the western Mediterranean Sea (Català et al. 2019), (h) SST record from the Arabian Sea (Sirocko et al. 1993), (i) SST record from the North Atlantic (Kim et al. 2004), (j) Siberian High intensity (Mayewski et al. 2004), (k) the estimated PGDW condition (l) and climate record of the Middle East (Issar, 2004) are represented. b): Comparison of summer and winter surface temperature change (in °C) in 30° N (Iranian Plateau) and 25° N (Arabian Peninsula and the Oman Sea) since the mid-Holocene.

Journal Pre-proof

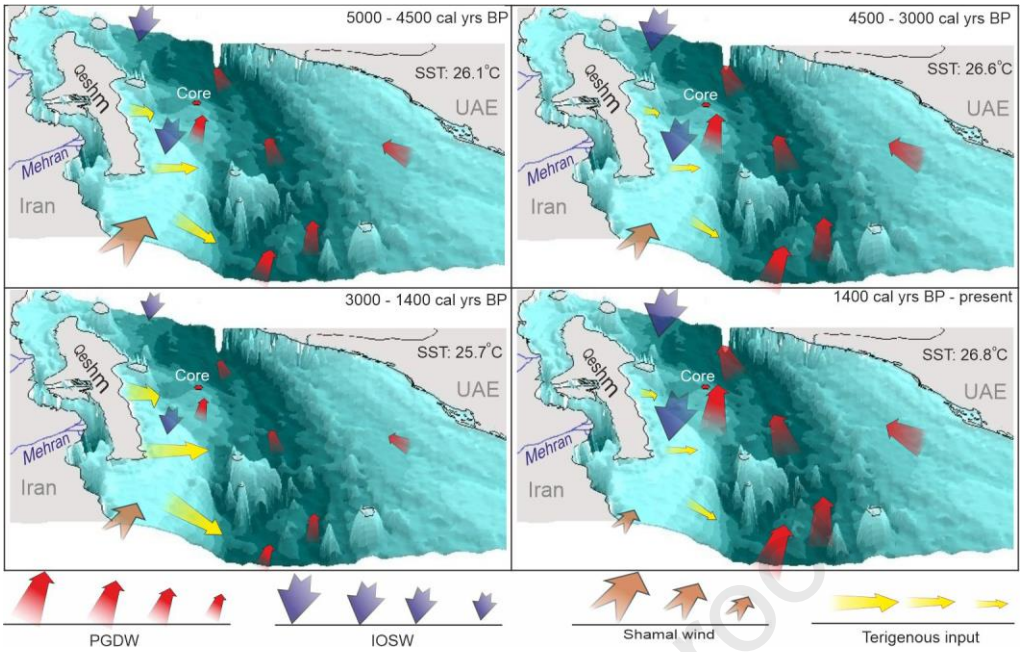
605 **4.2.2. Unit B: 4300 – 2000 cal yr BP**

606 This period begins with an abrupt increase in SST of the SH, as well as the
607 Mediterranean Sea (Català et al. 2019) likely due to solar irradiance (Mayewski et al. 2004).
608 Nonetheless, the mean annual SST of the Arabian Sea is lower than both above mentioned.
609 This significant warming is also documented in the Near East by a prolonged drought (Issar
610 2004). The high aeolian input, high salinity, and rise in evaporite minerals were detected around
611 4.3 cal kyr BP in lake sediments of Hamun-e Jazmurian suggesting a dry condition (Vaezi et
612 al. 2018). At the same time, Bronze Age civilization in the southeast and east of Iran evanesced.
613 Using palynology of a peat bog close to Konar Sandal archaeological site (150 km north of
614 SH), Gurjazkaite et al. (2018) detected a drought period ended at 3.8 cal kyr BP. Cullen et al.
615 (2000) indicated that climate deterioration in the Middle East around 4.2 cal kyr BP led to the
616 demise of the Akkadian Empire. Paleoceanography of the Red Sea indicates that terrigenous
617 input and SR in this period was lower than the periods before and after that. The destructive
618 effects of weakened ISM (expansion of summer season) may be considered as responsible for
619 climate deterioration in this warm period (Miller et al. 2016; Djamali et al. 2010).
620 Varying faunal and non-faunal indicators such as increasing MS value, sand content
621 and epifaunal communities as well as decreasing silt content demonstrate a gradual increase in
622 PGDW strength which may be attributed to an abrupt SST increase in the SH and its relatively
623 high discrepancy with the Arabian Sea (Fig. 6 and g). Since 3.5 cal kyr BP, SST started to
624 decline gradually which was accompanied by an increasing terrigenous input. Paleoclimate
625 researches suggest that southward migration of ITCZ has caused the higher ISM-induced
626 precipitations were replaced by lower MLW-induced Mediterranean winter precipitations
627 (Fleitmann et al. 2007; Hamzeh et al. 2006). The decreasing trend of the PG SST in this period
628 is in agreement with the gradual decrease in SST of the Red Sea and the Mediterranean Sea,
629 and also a decrease in the strength of the Siberian High (Mayewski et al. 1997). This wetter
630 condition is consistent with an increase in the water level of the Dead Sea and the Lake Van
631 (Wick et al., 2003; Frumkin et al. 1991), and enhancing Tigris and Euphrates discharge (Kay
632 and Johnson, 1981). In general, as the mean SST of this period is lower than that of Unit D
633 (the last 1450 years), and Arabian Sea SST slightly decreases (Fig. 6g) causing a decline in
634 SST contrast between the PG and the Arabian Sea, the variation magnitude of PGDW proxies
635 is relatively low. Relatively lower winter isolation (reduction of saline water originated from
636 northwest of the PG and the Arabian shallow shelf) compared to present time provides another
637 hint that PGDW intensity during this period was lower than that of today. Altogether, at this

time, the PGDW is rather weaker and terrigenous input is higher than that of the corresponding period of unit D.

4.2.3. Unit C: 2000 – 1450 cal yr BP

SST cooling, PGDW weakening and terrigenous input (and also SR) increasing trend, started about 1500 years earlier, reach their highest values in this period. Paleoclimate reconstruction indicates that SST from 3.5 to 1.5 cal kyr BP is about 2°C lower than that of today (Safarkhani et al. 2021). This SST variation trend is also traceable in the Arabian Sea, the Mediterranean Sea and the North Atlantic (Fig. 6g, h and i). Paleoclimate study in Khuran Estuary (north of Qeshm Island) demonstrates that during this time the discharge of the rivers inflowing to the Strait of Hormoz has been much higher than today (Hamzeh and Farahi Ghasr-Aboonasr, 2020). Miller et al. (2016) suggested a high amount of freshwater discharge and low dust input into the Oman Sea during this time. Arz et al. (2003) also indicated that during this time interval the river discharge in the Red Sea basin reached the maximum over the last 5000 years. During the same period, a climate optimum documented in various archives e.g., sediments of caves, lakes, and seas in the Middle East period (Bar-Matthews et al. 2003; Wick et al. 2003; Frumkin et al. 1991). It seems that, because summer insolation decreased and winter insolation was still lower than that of today (Fig. 6a) the evaporation rate (as the forcing factor of penetrating the IOSW (Reynolds, 1993)) decreased, and therefore, the overall PGDW intensity was relatively low (Fig. 7). This time of high river inflow and low-energy PGDW provided a favourable condition for the expansion of benthic foraminifera (mostly infaunal taxa such as *Bolivina*, *Ammonia*, *Bulimina* and *Lagena*).



661

662 **Fig. 7.** 3D map of the SH showing the intensity of inflowing surface currents, bottom currents, Shamal wind and
663 the amount of terrigenous input over the last 5000 years.

664

665 **4.2.4. Unit D: 1450 cal yr BP to present**

The highest average SST of the PG is recorded over the last 1450 year (mean: 26. 7°C), which is consistent with the general trend of increased SST in the neighbouring water bodies, such as the Arabian Sea, the Red Sea, and the Mediterranean Sea, which are all marked by notable fluctuations. This period is synchronous with a gradual and oscillating deterioration of the climate all over the Middle East (Issar 2004). Based on the isotopic composition of the stalagmites in Soreq Cave, Bar- Matthews et al. (2003) showed that the average annual precipitation over the eastern Mediterranean began to decrease sometime after 1400 cal yr BP. A relatively high SST in the area is the forcing factor for reinforcement of PGDW which has the strongest bottom currents during the last 5000 years. This is reinforced by the highest winter isolation in the Holocene, which possibly increases the outflow of saline water from the northwestern and southern shallow shelves, and by a decline in the intensity of Shamal winds (Felis et al. 2000) during winter which may increase the IOSW inflow. Although high energy bottom currents provide a harsh environment for benthic fauna, they bring oxygenated water together with phytodetritus particles for the persistence of foraminifera (mostly large epifaunal suspension feeders). After unit C, this unit comprises the most BFAR of the last 5000 years.

Journal Pre-proof

SST warming trend is disrupted by a prominent SST cooling (~700-600 cal yr BP) which can be traced back, with a multi-decade age difference, to the Mediterranean Sea. This period which led to an increase in the input of terrigenous sediments into the PG, taking the age uncertainties into account, appears to be related to the Little Ice Age (LIA) cold spell in the Northern Hemisphere. Such a condition has been also reported by Leroy et al. (2011) in Anzali and Amirkola lagoons (southern coasts of the Caspian Sea). A palynological investigation conducted by Miller et al. (2016) indicated a shift from desert to grassland vegetation, implying wetter conditions during the LIA in southern Iran. This short period is also recognizable by the reduction of the number of foraminifera, particularly epifaunal taxa. It may be attributed to a short time reduction in PGDW strength and higher terrigenous input.

5. Conclusions

The present paper, for the first time, reconstructs paleocurrent strength variations of PGDW in the SH and its connection with the paleoclimate of SW Asia. Since the mid-Holocene, precession-related increasing boreal winter insolation caused a long-term SST increase, while solar variability was responsible for short-term SST changes. During the periods of reduced SST, the bottom current energy of PGDW decreases and a notable increase occurs in river discharges into the area. Finer sediment deposition in a relatively low energy bottom provides a favourable environment for benthic foraminifera (dominated by infaunal taxa). Conversely, during the episodes of increased SST in the SH and warming in the surrounding lands which are associated with climate aridity in the Middle East and the Iranian Plateau, PGDW strength increases. The general SST warming in the PG is concordant with the winter insolation increase, and in turn, the decline in the inflow of cold air masses to the area. The periods of high winter isolation cause increasing outflow of saline water from the northwestern and southern shallow shelves and reducing the intensity of Shamal winds (Felis et al. 2000) which elevates the IOSW inflow. High energy bottom currents in these periods cause the domination of epifaunal foraminifera. However, these high DO and phytodetritus content bottom currents cause propagation of robust suspension feeder epifaunal taxa. Indeed, as Hamzeh and Farahi Ghasr-Aboonasr (2020) and Miller et al. (2016) concluded, the progressive global warming trend causing climate aridity (due to extending summer length) is linked to the increasing SST and PGDW intensification in the PG and SH basin.

Acknowledgements

This study is an integral part of a comprehensive study of the Persian Gulf Explorer research project, supported by the Iranian National Institute for Oceanography and Atmospheric Science, with financial support from Lorestan University. The authors would like to thank the crew staff of R/V Persian Gulf Explorer, especially Mr S. Sanjani and Dr A. Saleh as technical and scientific managers respectively.

References

Al-Ghadban, A.N., Abdali, F. and Massoud, M.S. (1998). Sedimentation rate and bioturbation in the Arabian Gulf. Environment International 24(1-2): 23-31.

Al-Said, T., Yamamoto, T., Madhusoodhanan, R., Al-Yamani, F. and Pokavanich, T. (2018). Summer hydrographic characteristics in the northern ROPME Sea Area: Role of ocean circulation and water masses. Estuarine, Coastal and Shelf Science 213: 18-27.

Amao, A.O., Kaminski, M.A., Rostami, M.A., Mahmudi-Gharaie, M.H., Lak, R. and Frontalini, F. (2019). Distribution of benthic foraminifera along the Iranian coast. Marine Biodiversity 49(2: 933-946.

Arz, H.W., Lamy, F., Patzold, J., Muller, P.J. and Prins, M. (2003). Mediterranean Moisture Source for an Early-Holocene Humid Period in the Northern Red Sea. Science 300: 118-121.

Azizpour, J., Chegini, V., Khosravi, M. and Einali, A. (2014). Study of the physical oceanographic properties of the Persian Gulf, Strait of Hormuz and Gulf of Oman based on PG-GOOS CTD measurements. Journal of the Persian Gulf 5(18): 37-48.

Baltzer, F. and Purser, B.H. (1990). Modern alluvial fan and deltaic sedimentation in a foreland tectonic setting: the lower Mesopotamian plain and the Arabian Gulf. Sedimentary Geology 67(3-4): 175-197.

Bar-Matthews, M., Ayalon, A., Gilmour, M., Matthews, A., Hawkesworth, C.J. (2003). Seaeland oxygen isotopic relationships from planktonic foraminifera and speleothems in the Eastern Mediterranean region and their implication for paleorainfall during interglacial intervals. Geochimica et Cosmochimica Acta 67: 3181-3199.

Basson, P.W., and Murray, J. (1995). Temporal variations in four species of intertidal foraminifera, Bahrain, Arabian Gulf. Micropaleontology 41: 69–76.

699 Berger, A., Loutre, M. F. (1991). Insolation values for the climate of the last 10 million years.
700 Quaternary Science Reviews 10: 297-317.
701 Blaauw, M., 2010. Methods and code for 'classical' age-modelling of radiocarbon
702 sequences. Quaternary Geochronology 5, 512-518.
703 Bower, A.S., Hunt, H.D. and Price, J.F. (2000). Character and dynamics of the Red Sea and
704 Persian Gulf outflows. Journal of Geophysical Research: Oceans 105(C3): 6387-6414.
705 Bruthans, J., Filippi, M., Geršl, M., Zare, M., Melková, J., Pazdur, A., Bosák, P. (2006).
706 Holocene marine terraces on two salt diapirs in the Persian Gulf, Iran: age, depositional
707 history and uplift rates. Journal of Quaternary Science: Published for the Quaternary
708 Research Association 21: 843–857.
709 Català, A. Cacho, I., Frigola, J., Pena, L.D. and Lirer, F. (2019) Holocene hydrography
710 evolution in the Alboran Sea: a multi-record and multi-proxy comparison. Climate pof the
711 Past 15: 927-942.
712 Cherif, O.H., Al-Ghadban, A.N., Al-Rifaiy, I.A. (1997) Distribution of foraminifera in the
713 Arabian Gulf. Micropaleontology 43: 253–280.
714 Cullen, H.M., deMenocal, P.B., Hemming, S., Hemming, G., Brown, F.H., Guilderson, T. and
715 Sirocko, F. (2000) Climate change and the collapse of the Akkadian empire: Evidence
716 from the deep sea. Geology 28(4), 379-382.
717 Diester-Haass, L. (1973). Holocene climate in the Persian Gulf as deduced from grain size and
718 petropod distribution. Marine Geology 14: 207- 223.
719 Djamali, M., Akhani, H., Andrieu-Ponel, V., Braconnot, P., Brewer, S., de Beaulieu, J.-L.,
720 Fleitmann, D., Fleury, J., Gasse, F., Guibal, F., Jackson, S.T., Lézine, A.-M., Médail, F.,
721 Ponel, P., Roberts, N., Stevens, L., 2010. Indian Summer Monsoon variations could have
722 affected the early-Holocene woodland expansion in the Near East. Holocene 20, 813-820.
723 Doose-Rolinski, H., Rogalla, U., Scheeder, G., Luckge, A. and von Rad, U. (2001). High-
724 resolution temperature and evaporation changes during the late Holocene in the
725 northeastern Arabian Sea. Paleoceanography 16(4): 358-367.
726 Evans, G., Murray, J.W., Biggs, H.E.J., Bate, R. and Bush, P.R. (1973). The oceanography,
727 ecology, sedimentology and geomorphology of parts of the Trucial Coast barrier island
728 complex, Persian Gulf. In The Persian Gulf (pp. 233-277). Springer, Berlin, Heidelberg.
729 Felis, T., Pätzold, J., Loya, Y., Fine, M., Nawar, A.H. and Wefer, G. (2000). A coral oxygen
730 isotope record from the northern Red Sea documenting NAO, ENSO, and North Pacific
731 teleconnections on Middle East climate variability since the year 1750, Paleoceanography,
732 15, 679– 694.

733 Fisher, R.A., Corbet, A.S., and Williams, C.B. (1943). The relation between the number of
734 species and the number of individuals in a random sample of an animal population. J.
735 Anim. Ecol. (1): 42–58.
736 Fleitmann, D., Burns, S.J., Mangini, A., Mudelsee, M., Kramers, J., Villa, I., Neff, U., Al-
737 Subbary, A.A., Buettner, A., and Hippler, D. (2007). Holocene ITCZ and Indian monsoon
738 dynamics recorded in stalagmites from Oman and Yemen (Socotra). Quaternary Science
739 Reviews 26: 170-188.
740 Frumkin, A., Magaritz, M., Carmi, I. and Zak, I. (1991). The Holocene climatic record of the
741 salt caves of Mount Sedom, Israel. The Holocene 1: 191–200.
742 Ghasemifar, E., Farajzadeh, M., Mohammadi, C. and Alipoor, E. (2020). Long-term change of
743 surface temperature in water bodies around Iran–Caspian Sea, Gulf of Oman, and Persian
744 Gulf–using 2001–2015 MODIS data. Physical Geography 41(1): 21-35.
745 Gurjazkaite, K., Routh, J., Djamali, M., Vaezi, A., Poher, Y., Beni, A.N., Tavakoli, V. and
746 Kylin, H. (2018). Vegetation history and human-environment interactions through the late
747 Holocene in Konar Sandal, SE Iran. Quaternary Science Reviews 194: 143-155.
748 Gupta, A.K., David M. Anderson, D.M. and Overpeck, J.T. (2003). Abrupt changes in the
749 Asian southwest monsoon during the Holocene and their links to the North Atlantic Ocean.
750 Nature 421(23): 354-357.
751 Haake. F. (1975). Miliolinen (Foram) in oberflachensedimenten des Persischen Golfes.
752 "Meteor" Forsch-Ergebnisse 21: 15–51.
753 Haake, F.W. (1970). Zur Tiefenverteilung von Miliolinen (Foram.) im Persischen Golf.
754 Paläontol Z 44: 196–200.
755 Haghipour, A., Fontugne, M. (1993). Quaternary uplift of Qeshm Island (Iran). Comptes
756 Rendus de l'Académie des Sciences, Paris 317 (II): 419–424.
757 Hamzeh, M.A. in press. Environmental implications of the distribution and physical
758 characteristics of surface sediments in the northern Persian Gulf. Geo-Marine Letters.
759 Hamzeh, M.A., Gharaie, M.H.M., Lahijani, H.A.K., Djamali, M., Harami, R.M. and Beni, A.N.
760 (2016). Holocene hydrological changes in SE Iran, a key region between Indian Summer
761 Monsoon and Mediterranean winter precipitation zones, as revealed from a lacustrine
762 sequence from Lake Hamoun. Quaternary International 408: 25-39.
763 Hamzeh, M.A. and Farahi Ghasr-Aboonasr, S. (2020). Palaeoenvironmental changes in the
764 Khuran Estuary of SE coastal Iran during the last two millennia, based on the analysis of
765 a sediment core. Palaeogeography, Palaeoclimatology, Palaeoecology 542: 109563.

Journal Pre-proof

766 Haynes, J.R., (1981). Foraminifera. McMillan Publishers LTD, London and Basingstoke,
767 475p.
768 Heiri, O., Lotter, A.F. and Lemcke, G. (2001). Loss on ignition as a method for estimating
769 organic and carbonate content in sediments: reproducibility and comparability of results.
770 Journal of Paleolimnology 25: 101-110.
771 Herguera, J. C. (1992). Deep-sea benthic foraminifera and biogenic opal: Glacial to postglacial
772 productivity changes in the western equatorial Pacific, Marine Micropaleontology 18: 79-
773 98.
774 Hollister, C. D., & Heezen, B. C. (1972). Geologic effects of ocean bottom currents: Western
775 North Atlantic. In: A. L. Gordon (Ed.), Studies in physical oceanography (Vol. 2, pp. 37–
776 66). New York: Gordon and Breach.
777 Hunter, J.R. (1986). The physical oceanography of the Arabian Gulf: a review and theoretical
778 interpretation of previous observations. In: Marine Environment and Pollution.
779 Proceedings 1st Arabian Gulf Conference on Environmental Pollution. Kuwait University,
780 Kuwait, pp. 1-23.
781 IWRMC (2016). Report on Water Resources Yields in Bandar Abbas District (code: 2801),
782 Feb. 2016. Report no. 300-28-RPT-WB-Ba-02. Sangab Zagros Consulting Engineers, Iran
783 Water Resource Management Co (70p).
784 Issar, A.S. (2004). Climate Changes during the Holocene and their Impact on Hydrological
785 Systems, Cambridge University Press, Cambridge.
786 Johns, W.E., Yao, F. and Olson, D.B. (2003). Observations of seasonal exchange through the
787 Straits of Hormoz and the inferred heat and freshwater budgets of the Persian Gulf. Journal
788 of Geophysical Research 108(12): 1-18.
789 Kassler, P. (1973). The structural and geomorphic evolution of the Persian Gulf. In The Persian
790 Gulf (pp. 11-32). Springer, Berlin, Heidelberg.
791 Kay, P.A. and Johnson, D.L. (1981). Estimation of Tigris-Euphrates streamflow from regional
792 paleoenvironmental proxy data. Climatic Change 3: 251-263.
793 Khosravi, M., Siadatmousavi, S.M., Vennell, R., Chegini, V. (2018) The transverse dynamics
794 of flow in a tidal channel within a greater strait. Ocean Dynamics 10236-017-1127-3
795 Kim, J.-H., Rimbu, N., Lorenz, S.J., Lohmanna, G., Nam, S.-I., Schoutene, S., Ruhlemannf, C.
796 and Schneiderg, R.R. (2004) North Pacific and North Atlantic sea-surface temperature
797 variability during the Holocene. Quaternary Science Reviews 23: 2141-2154.
798 Kodera, K. (2004). Solar influence on the Indian Ocean Monsoon through dynamical
799 processes. Geophysical Research Letters 31(24): L24209.

800 Konert, M., Vandenberghe, J. (1997). Comparison of laser grain size analysis with pipette and
801 sieve analysis: a solution for the underestimation of the clay fraction. Sedimentology 44:
802 523-535.
803 Kucera, M. (2007). Planktonic foraminifera as tracers of past oceanic environments, In:
804 Developments in marine geology 1: 213-262.
805 Leroy, S.A.G., Lahijani, H.A.K., Djamali, M., Naqinezhad, A., Moghadam, M.V., Arpe, K.,
806 Shah-Hosseini, M., Hosseindoust, M., Miller, C.S., Tavakoli, V., Habibi, P. and Naderi
807 Beni, M. (2011). Late Little Ice Age palaeoenvironmental records from the Anzali and
808 Amirkola Lagoons (south Caspian Sea): Vegetation and sea level changes.
809 Palaeogeography, Palaeoclimatology, Palaeoecology 302: 415-434.
810 Liu, Z., Brady, E., and Lynch-Stieglitz, L. (2003). Global ocean response to orbital forcing in
811 the Holocene, Paleoceanography, 18(2): 1041, doi:10.1029/2002PA000819.
812 Loeblich, A.R., Tappan, H. (1988). Foraminiferal Genera and Their Classification. Springer
813 Science Business Media New York (2045p).
814 Lorenz, M., Klingbeil, K. and Burchard, H. (2020). Numerical study of the exchange flow of
815 the Persian Gulf using an extended total exchange flow analysis framework. Journal of
816 Geophysical Research: Oceans 125(2). doi:10.1029/2019JC015527.
817 Lorenz, S.J., Kim, J.H., Rimbu, N., Schneider, R.R. and Lohmann, G. (2006). Orbitally driven
818 insolation forcing on Holocene climate trends: Evidence from alkenone data and climate
819 modeling. Paleoceanography, 21(1). PA1002, doi:10.1029/2005PA001152.
820 Lutze, G. F., and Altenbach, A. (1988). Rupertina stabilis (WALLICH), a highly adapted,
821 suspension feeding foraminifer. Meyniana, 40: 55–69.
822 Majidzadeh, Y. 2003, Jiroft: The Earliest Oriental Civilization: Printing and Publishing of the
823 Ministry of Culture and Islamic Guidance, Tehran 69–103.
824 Mayewski, P.A., Meeker, L.D., Twickler, M.S., Lyons, W.B., and Prentice, M. (1997). Major
825 features and forcing of high-latitude northern hemisphere atmospheric circulation using a
826 110,000-year-long glaciochemical series. J. Geophys. Res 102: 26,345 - 26,366.
827 Mayewski, P.A., Rohling, E.E., Stager, J.C., Karlén, W., Maasch, K.A., Meeker, L.D.,
828 Meyerson, E.A., Gasse, F., van Kreveld, S. and Holmgren, K. (2004). Holocene climate
829 variability. Quaternary Research 62(3)): 243-255.
830 McCave, I.N. 2007. Deep-sea sediment deposits and properties controlled by
831 currents. Developments in Marine Geology 1: 19-62.
832 Milankovitch, M.K. (1941). Kanon der Erdbestrahlung und seine Anwendung auf das
833 Eiszeitenproblem. Royal Serbian Academy Special Publication 133, pp.1-633.

Journal Pre-proof

834 Miller, C.S., Leroy, S.A.G., Collins, P.E.F. and Lahijani, H.A.K. (2016). Late Holocene
835 vegetation and ocean variability in the Gulf of Oman. Quaternary Science Reviews 143:
836 120-132.
837 Molinaro, M., Guezou, J.C., Leturmy, P., Eshraghi, S., de Lamotte, D.F. (2004). The origin of
838 changes in structural style across the Bandar Abbas syntaxis, SE Zagros (Iran). Mar. Pet.
839 Geol. 21, 735–752.
840 Mudroch, A., Azcue, J.M., Mudroch, P. (1997). Manual of Physico-Chemical Analysis of
841 Aquatic Sediments. Lewis Publishers, CRC Press, USA (287p).
842 Murray, J.W. (1965). The foraminiferida of the Persian Gulf. Part I. Rosalina adhaerens sp.
843 nov. Annals and Magazine of Natural History, 8(86): 77-79.
844 Murray, J. (1966). The Foraminiferida of the Persian Gulf. 5. The shelf off the trucial coast.
845 Palaeogeogr Palaeoclimatol Palaeoecol 2: 267–278
846 Murray, J. (1970). The Foraminiferida of the Persian Gulf: 6. Living forms in the Abu Dhabi
847 region. J Nat Hist 4: 55–67
848 Murray, J.W., 2006. Ecology and Applications of Benthic Foraminifera. Cambridge University
849 Press (426p).
850 Nabavi, S.M.B., Moosapanah, S.G.R., Rajab Zadeh Ghatrami, E., Ghayyem Ashrafi, M. and
851 Nabavi, S.N. (2014). Distribution, Diversity and Abundance of Benthic Foraminifera of
852 the Northwstern Persian Gulf. Journal of the Persian Gulf 5(16): 15-26.
853 Olsen, J., Ascough, P., Lougheed, B.C., Rasmussen, P. (2017). Radiocarbon dating in estuarine
854 environments. In: Applications of Paleoenvironmental Techniques in Estuarine Studies.
855 Springer, pp. 141–170.
856 Parker, J.H., Gischler, E. (2015). Modern and relict foraminiferal biofacies from a carbonate
857 ramp, offshore Kuwait, northwest Persian Gulf. Facies 61: 1-22.
858 Pfannkuche, O., Sommer, S. and Kähler, A. (2000). Coupling between phytodetritus deposition
859 and the small-sized benthic biota in the deep Arabian Sea: analyses of biogenic sediment
860 compounds. Deep Sea Research Part II: Topical Studies in Oceanography 47(14): 2805-
861 2833.
862 Pirazzoli, P.A., Reyss, J.L., Fontugne, M., Haghipour, A., Hilgers, A., Kasper, H.U., Nazari,
863 H., Preusser, F. and Radtke, U. (2004). Quaternary coral-reef terraces from Kish and
864 Qeshm Islands, Persian Gulf: new radiometric ages and tectonic implications. Quaternary
865 International 120(1): 15-27.

Potts, D.T., Lamberg-Karlovski, C., Pittman, H., Kohl, P.L. (2001). Excavations at Tepe Yahya, Iran, 1967–1975: the third millennium: Peabody Museum of Archaeology, v. 45, p. 85–146.

Pous, S., Lazure, P., and Carton, X. (2015). "A model of the general circulation in the Persian Gulf and in the Strait of Hormuz: Intraseasonal to interannual variability." Continental Shelf Research 94, 55-70.

Purser, B.H. and Seibold, E. (1973). The principal environmental factors influencing Holocene sedimentation and diagenesis in the Persian Gulf. In The Persian Gulf (pp. 1-9). Springer, Berlin, Heidelberg.

Regard, V., Bellier, O., Braucher, R., Gasse, F., Bourlès, D., Mercier, J., Thomas, J.C., Abbassi, M.R., Shabanian, E. and Soleymani, S. (2006). ^{10}Be dating of alluvial deposits from Southeastern Iran (the Hormoz Strait area). Palaeogeography, Palaeoclimatology, Palaeoecology 242(1-2): 36-53.

Reimer, P.J., Austin, W.E., Bard, E., Bayliss, A., Blackwell, P.G., Ramsey, C.B., Butzin, M., Cheng, H., Edwards, R.L., Friedrich, M. and Grootes, P.M. (2020). The IntCal20 Northern Hemisphere radiocarbon age calibration curve (0–55 cal kBP). Radiocarbon, 62(4), pp.725-757.

Reynolds, R.M. (1993). Physical Oceanography of the Persian Gulf, Strait of Hormuz, and the Gulf of Oman — Results from the Mt. Mitchell Expedition. Marine Pollution Bulletin 27: 35-59.

Rimbu, N., Lohmann, G., Lorenz, S.J., Kim, J.H. and Schneider, R.R. (2004). Holocene climate variability as derived from alkenone sea surface temperature and coupled ocean-atmosphere model experiments. Climate Dynamics, 23(2), 215-227.

Safarkhani, E., Yarahmadi, D., Hamzeh, M.A., and Sharafi, S. (2021). Reconstruction of the Persian Gulf SST variability over the last five millennia. Quaternary International. Doi: 10.1016/j.quaint.2021.01.028

Saher, M.H., Jung, S.J.A., Elderfield, H., Greaves, M.J. and Kroon, D. (2007). Sea surface temperatures of the western Arabian Sea during the last deglaciation. Paleoceanography 22 .

Saidova, K.M. (2010). Benthic foraminifer communities of the Persian Gulf. Oceanology 50: 61–66.

Saleh, A., Abtahi, A., Mirzaei, N., Chen, A., Ershadifar, H., Ghaemi, M., Hamzehpour, A., Abedi, E. (in press). Hypoxia in the Persian Gulf and the Strait of Hormuz. Marine Pollution Bulletin.

900 Salvatori, S. and Vidale, M. (1982). A brief surface survey of the Protohistoric site of Shahdad
901 (Kerman, Iran): Rivista di Archeologia VI 6: 5–10.
902 Sarnthein, M. (1972). Sediments and history of the postglacial transgression in the Persian Gulf
903 and northwest Gulf of Oman. Marine geology, 12(4): 245-266.
904 Schönfeld, J. (1997). The impact of the Mediterranean Outflow Water (MOW) on benthic
905 foraminiferal assemblages and surface sediments at the southern Portuguese continental
906 margin. Marine Micropaleontology 29: 211–236.
907 Schönfeld, J. (2002a). Recent benthic foraminiferal assemblages in deep high-energy
908 environments from the Gulf of Cadiz (Spain). Micropaleontology 44: 141–162.
909 Schönfeld, J. (2002b). A new benthic foraminiferal proxy for near-bottom current velocities in
910 the Gulf of Cadiz, northeastern Atlantic Ocean. Deep-Sea Research I, 49: 1853–1875.
911 Sen Gupta, B. K., Smith, L. E., & Lobegeier, M. K. (2006). Attachment of Foraminifera to
912 vestimentiferan tubeworms at cold seeps Refuge from sea-floor hypoxia and sulfide
913 toxicity. Marine Micropaleontology 62(1): 1–6.
914 Sheppard, C., Al-Husiani, M., Al-Jamali, F., Al-Yamani, F., Baldwin, R., Bishop, J., Benzoni,
915 F., Dutrieux, E., Dulvy, N.K., Durvasula, S.R.V. and Jones, D.A. (2010). The Gulf: a
916 young sea in decline. Marine Pollution Bulletin 60(1): 13-38.
917 Shimmield, G., Derrick, S., Mackensen, A., Grobe, H., & Pudsey, C. (1994). The history of
918 barium, biogenic silica and organic carbon accumulation in the Weddell Sea and Antarctic
919 Ocean over the last 150,000 years. In: R. Zahn, T. F. Pedersen, M. A. Kaminski & L.
920 Labeyrie (Eds), Carbon cycling in the glacial ocean: Constraints on the ocean's role in
921 global change (pp. 555–574). Springer Verlag.
922 Sirocko, F., Sarnthein, M., Erlenkeuser, H., Lange, H., Arnold, M., Duplessy, J.C. (1993).
923 Century-scale events in monsoonal climate over the past 24,000 years. Nature 364, 322–
924 324.
925 Southon, J., Kashgarian, M., Fontugne, M., Metivier, B. and Yim, W.W. (2002) Marine
926 reservoir corrections for the Indian Ocean and Southeast Asia. Radiocarbon 44(1), 167-
927 180.
928 Taghipour, S., and Taghipour, B. (2009). Mineralogical studies of metasomatic minerals within
929 volcanic rocks of High Zagros salt domes. Iranian Journal of Crystallography and
930 Mineralogy 4(17): 535-550.
931 Tosi, M. (1983). Prehistoric Sistan: Reports and Memoirs, v. 19, IsMEO, Rome.
932 Vaezi, A., Ghazban, F., Tavakoli, V., Routh, J., Beni, A.N., Bianchi, T.S., Curtis, J.H. and
933 Kylin, H. (2019). A Late Pleistocene-Holocene multi-proxy record of climate variability

in the Jazmurian playa, southeastern Iran. Palaeogeography, Palaeoclimatology, Palaeoecology 514: 754-767.

Wick, L., Lemcke, G. and Sturm, M. (2003). Evidence of Lateglacial and Holocene climatic change and human impact in eastern Anatolia: high-resolution pollen, charcoal, isotopic and geochemical records from the laminated sediments of Lake Van, Turkey. The Holocene 13(5): 665-675.

Wyrtki, K. 1971. Oceanographic atlas of the International Indian Ocean Expedition. Nat. Sci. Found. Washington D.C., 531 p.

Yao, F., and Johns, W.E. (2010). A HYCOM modeling study of the Persian Gulf: 2. Formation and export of Persian Gulf Water. Journal of Geophysical Research: Oceans 115(C11).

Zhong, Y., Chen, Z., Li, L., Liu, J., Li, G., Zheng, X., Wang, S. and Mo, A. (2017). Bottom water hydrodynamic provinces and transport patterns of the northern South China Sea: Evidence from grain size of the terrigenous sediments. Continental Shelf Research 140: 11-26.

Journal Pre-proof

963 # Appendices

964 A1: List of benthic foraminiferal taxa (order, family genus and species) identified from the core T2S3

Order	Family	Genus	Species
Astrorhizida	Rhabdamminidae	*Marsipella*	sp1
Lagenida	Lagenidae	*Lagena*	*perlucida, semistriata*
	Ellipsolagenidae	*Fissurina*	*bispinata, lucida*
		Oolina	sp1
	Nodosariidae	*Pyramidulina*	sp1
Lituolida	Trochamminidae	*Trochammina*	sp1, sp2
Miliolida	Cribrolinoididae	*Adelosina*	*honghensis, laevigata*
	Hauerinidae	*Quinqueloculina*	*bosciana, limbate, quinquecarinata, seminula,* sp5, sp6, sp7, sp8, sp9
		Sigmoilopsis	sp1, sp2
		Triloculina	*tricarinata, trigonula, wiesneri*
	Ophthalmidiidae	*Spirophthalmidium*	sp1
	Spiroloculinidae	*Spiroloculina*	*communis, depressa, elegantisima*
	Clornuspiridae	*Cornuspira*	*involvens*
Rotaliida	Ammoniidae	*Ammonia*	*beccarii, tepida, faceta,* sp4
		Asterorotalia	*dentata, milletti*
		Challengerella	*Bradyi*
	Anomalinidae	*Hanzawaia*	*leroyi, tagaensis*
	Bolivinitidae	*Bolivina*	*dilatata, dottiana, foxenensis, spathulata, striatula, translucens,* sp7, sp8.
		Fursenkoina	sp1
	Buliminidae	*Bulimina*	*Marginate,* sp2
	Cancrisidae	*Cancris*	*oblongus, auriculus*
	Cassidulinidae	*Cassidulina*	*laevigata*
	Cibicididae	*Cibicides*	*lobatulus*
	Elphidiidae	*Cribroelphidium*	*excavatum*
		Elphidium	*advenum, fichtellianum, hispidulum.*
	Globorotaliidae	*Globorotalia*	sp1
	Nonionidae	*Nonion*	sp1, sp2, sp3
	Planorbulinidae	*Hyalinea*	sp1
	Rosalinidae	*Rosalina*	sp1
	Trimosinidae	*Trimosina*	sp1
Textulariida	Textulariidae	*Textularia*	*bocki, conica, earlandi, foliacea,* sp5, sp6

965

Journal Pre-proof

Journal Pre-proof

Highlights:

- During the last 5000 years, PGDW intensity has been under influence of the continental climate of SW Asia and the Arabian Sea SST.
- During the periods of increased SST (4500 to 3000 and 1400 cal yr BP to present), bottom current energy of the Strait of Hormoz increased and a notable decrease occurred in river discharges.
- Although high energy bottom currents provide a hostile environment for the benthic fauna, it causes domination of suspension feeder epifaunal foraminifera by carrying high DO content bottom waters.

Journal Pre-proof

Journal Pre-proof

Declaration of interests

The authors declare that they have no known competing financial interests or personal relationships that could have appeared to influence the work reported in this paper.

Journal Pre-proof